https://doi.org/10.5194/egusphere-2024-959
Preprint. Discussion started: 6 May 2024

Evaluation of the WRF-Chem Performance for gaseous pollutants over the United Arab Emirates.

Yesobu Yarragunta[1], Diana Francis[1*], Ricardo Fonseca[1] and Narendra Nelli[1]

[1] Environmental and Geophysical Sciences (ENGEOS) Lab, Khalifa University of Science and Technology, P. O. Box 127788, Abu Dhabi, United Arab Emirates

Correspondence to: Diana Francis (diana.francis@ku.ac.ae)

Abstract

This study presents a comprehensive evaluation of the Weather Research and Forecasting model coupled with Chemistry (WRF-Chem) in simulating meteorological parameters and concentrations of gaseous pollutants across the United Arab Emirates (UAE) for the months of June and December 2018, representing the contrasting climatic conditions of summer and winter. The assessment of WRF-Chem performance involved comparisons with ground-based observations for meteorological parameters and satellite retrievals from the TROPOspheric Monitoring Instrument (TROPOMI) for gaseous pollutants. The assessment of gaseous pollutants using the WRF-Chem model revealed distinct patterns in the estimation of pollutant levels across different areas and seasons. The comparison with TROPOMI column concentration revealed the model's strengths in simulating tropospheric NO_2 and total O_3 spatio-temporal patterns, although it had deficiencies in modelling the total CO column concentrations. The model exhibited a strong correlation with TROPOMI retrievals, with correlation coefficients ranging between 0.71 and 0.95 for summer and 0.86 to 0.94 for winter among these gaseous pollutants. It tended to slightly overestimate NO_2 levels, with a higher discrepancy observed in summer (0.24×10^{15} molecules/cm^2) compared to winter (0.19×10^{15} molecules/cm^2). When comparing WRF-Chem to TROPOMI-CO data, the discrepancies were more pronounced, showing an overestimation of 0.48×10^{18} molecules/cm^2 in summer and a significant underestimation of 1.13×10^{18} molecules/cm^2 in winter. The model consistently underestimated ozone levels in both seasons, by 0.15×10^{18} and 0.20×10^{18} molecules/cm^2, respectively. Meteorological evaluations revealed the model's tendency to underestimate the 2-m temperature in summer and overestimate it in winter, with mean biases ranging from -2.17

https://doi.org/10.5194/egusphere-2024-959
Preprint. Discussion started: 6 May 2024

to +1.19 °C and a Root Mean Square Error in the range of 0.8 to 5.9 °C among the stations. The model showed enhanced performance for the 10-m wind speed and downward shortwave radiation flux, reflecting advancements over previous studies. Therefore, the WRF-Chem model effectively simulates key meteorological parameters and pollutants over the UAE, demonstrating significant regional-scale prediction skills. Areas for further model refinement are also identified and discussed. Integrating model predictions with satellite and ground-based data is emphasized for advancing air quality monitoring and enhancing predictive accuracy of atmospheric pollutants in this region.

Keywords: Air quality modelling, gaseous pollutants, TROPOMI satellite retrievals, WRF-Chem, UAE.

Key points:

- First high-resolution WRF-Chem air quality modelling study over the United Arab Emirates (UAE)
- WRF-Chem's ability to simulate meteorological parameters and pollutant levels over the UAE is assessed during summer and winter in 2018.
- The model showed a strong correlation with TROPOMI satellite data, achieving correlation coefficients of 0.71-0.95 in summer and 0.86-0.94 in winter for different gaseous pollutants.
- Lower model skill in simulating total CO columns, in contrast to the more accurate modelling of tropospheric NO_2 and total O_3 columns as compared to TROPOMI data.
- Meteorological analysis revealed a tendency to underestimate surface temperature by 0.5 °C in summer and overestimate it by 1.3 °C in winter.
- Surface wind speed is overestimated by 0.1-0.9 m/s in both seasons across various regimes.

https://doi.org/10.5194/egusphere-2024-959
Preprint. Discussion started: 6 May 2024

1. Introduction

The United Arab Emirates (UAE), a federation of seven emirates, has undergone rapid urbanization and industrialization over the last five decades, which has had a profound impact on its air quality (Ramadan, 2015). The major factors affecting air quality in the UAE include emissions from industrial activities, vehicular traffic, construction projects, and occasionally, natural phenomena such as dust storms, which are quite prevalent in the region due to its desert climate (Environment Agency – Abu Dhabi, 2018; Francis et al., 2020; 2022b; Karagulian et al., 2019). The rapid economic growth of the UAE, especially in cities like Dubai and Abu Dhabi, has led to a surge in energy demand and desalinated water, largely met through the burning of fossil fuels (Shahbaz et al., 2014). This has resulted in increased emissions of pollutants like oxides of nitrogen (NOx), sulfur dioxide (SO_2), particulate matter (PM), and volatile organic compounds (VOCs). Moreover, the heavy traffic in urban areas contributes to the elevated levels of ground-level ozone and particulate pollution (Abuelgasim & Farahat, 2020; Li et al., 2010). Understanding the dynamics of air quality in the UAE involves considering both the environmental challenges posed by rapid development and the steps being taken to mitigate these impacts. The pursuit of balancing economic growth with environmental sustainability is central to this discourse. This area of study is not only vital for ensuring the health and well-being of the population but also plays a crucial role in the UAE's vision for a sustainable future.

The swift urban expansion in the UAE could intensify air pollution sources. With surface observations sparse in this region, satellite remote sensing becomes a crucial method for air quality monitoring (Chudnovsky et al., 2014; Fonseca et al., 2023; Francis et al., 2023). What is more, satellite measurements themselves fall short in clarifying the different atmospheric processes responsible for peak pollution levels. Consequently, integrating chemistry transport models with satellite-derived and ground-based observations can significantly improve our understanding of pollutant emissions, distribution, transport, and transformation in the targeted regions (Eltahan et al., 2018; Li et al., 2018; Yarragunta et al., 2020; Yin et al., 2021). Air quality (AQ) modelling is dedicated to unravelling the complicated aspects of atmospheric chemistry and transport across both global and regional levels, as explored in numerous studies conducted around the world (Emmons et al., 2010; Kumar et al., 2011, 2018; Tie et al., 2001; Yarragunta et al., 2019, 2020, 2021). Despite facing limitations due to the often low spatial and temporal resolution of observational data, AQ models effectively generate detailed air quality

https://doi.org/10.5194/egusphere-2024-959
Preprint. Discussion started: 6 May 2024

information for remote regions. They predict the formation and removal of air pollutants and facilitate a thorough examination of the transport and photo-chemical transformation of trace gases following their emission into the atmosphere (Archer-Nicholls et al., 2015; Georgiou et al., 2018; Nhu et al., 2021; Sicard et al., 2021). They are also employed globally for operational air quality forecasting (Jena et al., 2021; Koo et al., 2012; Kumar et al., 2012, 2021; Srinivas et al., 2016; Zhang et al., 2012). Air quality models are categorized into two types: 'fully coupled' models, which integrate interactions between chemistry and meteorology, and 'offline' models, where chemistry and meteorology simulations are conducted independently (Gao & Zhou, 2024). Some of state of the art AQ models include the Weather Research and Forecasting (WRF) model coupled with chemistry (WRF-Chem; Grell et al., 2005; Skamarock et al., 2008), WRF-Chem-MADRID (Model of Aerosol Dynamics, Reaction, Ionization and Dissolution, Zhang et al., 2010), CESM2 (Community Earth System Model version 2, Emmons et al., 2020), CHIMERE (Menut et al., 2021), LOTOS-EUROS(v2.0) (Long Term Ozone Simulation European Operational Smog, Manders et al., 2017) and COSMO/MESSy (Consortium for Small Scale Modelling/ Modular Earth Submodel System, Kerkweg & Jöckel, 2012). However, before using these AQ models for future applications, it is crucial to conduct thorough evaluations to assess the quality of their simulations. The AQ model chosen for the current study is the WRF-Chem with its foundational meteorological component, WRF.

The majority of studies conducted in the UAE and similar arid regions have primarily focused on evaluation of meteorological parameter including temperature, humidity, wind, and solar radiation (Parajuli et al., 2019; Nelli et al., 2020; Fonseca et al., 2020, 2021) with a few others investigating the particulate matter dynamics, especially mineral dust. For instance, Ukhov et al., (2021) noted inaccuracies in the WRF-Chem model related to the GOCART aerosol module, affecting $PM_{2.5}$ and PM_{10} diagnostics. Karagulian et al., (2019) highlighted the effectiveness of integrating WRF-chem model simulations with satellite and ground observations to understand and predict the impact of severe dust storms on air quality. Karumuri et al., (2022) reported significant air quality changes due to COVID-19 lockdown measures, with reduced trace gas concentrations but increased particulate matter from dust activities, the latter stressed by Francis et al. (2022a) who attributed it to changes in the atmospheric circulation. Moreover, Parajuli et al., (2022; 2023) utilized high-resolution WRF-Chem simulations and advanced aerosol schemes to analyse the dust and rainfall dynamics, providing insights into the direct and indirect effects of dust on rainfall which aids in better regional water resource planning through accurate rainfall predictions. However, no

https://doi.org/10.5194/egusphere-2024-959
Preprint. Discussion started: 6 May 2024

assessment to date for the gaseous pollutants model performance over the region despite the complex dynamics between anthropogenic and natural factors in air quality management and the necessity of tailored model configurations for accurate environmental assessments in arid regions.

This study represents the first evaluation of the WRF-Chem model in the region, specifically examining concentrations of gaseous pollutants along with crucial meteorological parameters relevant to air quality studies. The primary objective of this study is twofold:

- Evaluate the WRF-Chem's ability to replicate meteorological conditions. This involves comparing the model's simulation of temperature, wind speed, downward short-wave radiation and boundary layer height against ground-based observations and data from the ERA5 (Hersbach et al., 2020) reanalysis.
- Assess the model's performance in simulating concentrations of gaseous pollutants, specifically NO_2, O_3, and CO. The skill of the WRF-Chem in simulating these pollutants is evaluated by comparing its simulations against data from the TROPOspheric Monitoring Instrument (TROPOMI; Veekfind et al., 2012) on the Sentinel-5 Precursor satellite.

The structure of the paper is as follows: Section 2 describes the configuration of the WRF-Chem considered in this work. Section 3 elaborates on the methodology and datasets used in this study. Section 4 provides a comprehensive assessment of the WRF-Chem's simulated data with observational datasets, reanalysis and satellite-derived products. Section 5 concludes by outlining the main findings.

2. WRF-Chem configuration

The central objective of this study is to apply a regional chemistry/dynamical model to simulate the atmospheric conditions and transport of pollutants in the UAE, whose forecasts will be evaluated against in-situ, space-based measurements and a state-of-the-art reanalysis dataset. To this end, the WRF-Chem version 4.3.1 is employed. WRF-Chem is a mesoscale regional chemistry transport model, developed by the National Oceanic and Atmospheric Administration (NOAA) Earth System Research Laboratory (ESRL), and has been contributed to by the global science community. In WRF-Chem, air quality components and meteorological

https://doi.org/10.5194/egusphere-2024-959
Preprint. Discussion started: 6 May 2024

components are predicted simultaneously using the same grid coordinates, transport, timestep, and sub-grid scale physics. A detailed description of the model is found in Grell et al., (2005) and Skamarock et al., (2008). The physics schemes employed in the simulations are the Rapid Radiative Transfer Model for Global Circulations Models (RRTMG) for radiation parametrization of both short and long wave radiation (Iacono et al., 2008), the cloud microphysics is represented by the Morrison 2-moment (Morrison et al., 2009), and the Kain-Fritsch scheme is used for convective parameterisation (Kain, J.S, 2004). The Unified Noah model is used to represent the land surface model (Tewari et al., 2004) with an improved representation of soil texture and land use/land cover (LULC) over the UAE (Temimi et al., 2020). The boundary layer dynamics are represented by the Yonsei University (YSU) scheme (Hong, 2010). Other chosen physics schemes are listed in Table 1. Simulated mesoscale meteorology is kept in line with analysed meteorology through spectral nudging to the National Centre for Environmental Prediction (NCEP) Global Forecast System (GFS) analyses used to drive the model, in an attempt to limit errors in the mesoscale transport. During the simulations, horizontal and vertical wind, potential temperature and water vapour mixing ratio are nudged to GFS analyses in all model layers above the planetary boundary layer on a time-scale of 6 hours. Meteorological conditions were initialised by NCEP GFS 6-hourly analyses at 0.25° resolution.

This study utilised the Model for Ozone and Related Chemical Tracers, version 4 (MOZART-4) chemical mechanism for calculating gas-phase chemistry which includes 81 chemical species with 159 gas-phase reactions and 38 photolysis processes (Emmons et al., 2010). Aerosol chemistry is represented by the Goddard Chemistry Aerosol Radiation and Transport (GOCART; Chin et al., 2002), along with the Tropospheric, Ultraviolet and Visible (TUV) full photolysis scheme (Madronich, 1987; Tie, 2003), which deploys climatological O_3 and O_2 columns. Dry deposition was calculated using Wesely (1989). Anthropogenic emissions were taken from the Emission Database for Global Atmospheric Research version 5 (EDGARv5) at 0.1 × 0.1° horizontal resolution (Crippa et al., 2020). Emissions include SO_2, NOx, CO, NMVOC, NH_3, black carbon (BC) and organic carbon (OC). Biogenic emissions were calculated online by the Model of Emissions of Gases and Aerosol from Nature (MEGAN; Guenther et al., 2012). Model simulation uses CAM-chem model results as chemical boundary conditions (BCs) for the outer domain D01 and initial conditions (ICs) for all domains (Emmons et al., 2020). In this present work, we run the WRF-Chem model using the aforementioned physical and chemical processes on the three nested domains with

https://doi.org/10.5194/egusphere-2024-959
Preprint. Discussion started: 6 May 2024

horizontal resolutions 27-, 9- and 3-km corresponding to 283×205, 271×193 and 256×178 grid points and 45 vertical layers. The outermost domain covers the vast majority of the Middle East and surrounding region while the innermost domain covers the entire UAE (Fig. 1(a)). The analysis in this research article exclusively utilizes results from the inner domain (D03). The spatial distribution of ground-based observations from NCM are depicted in Fig. 1(b).

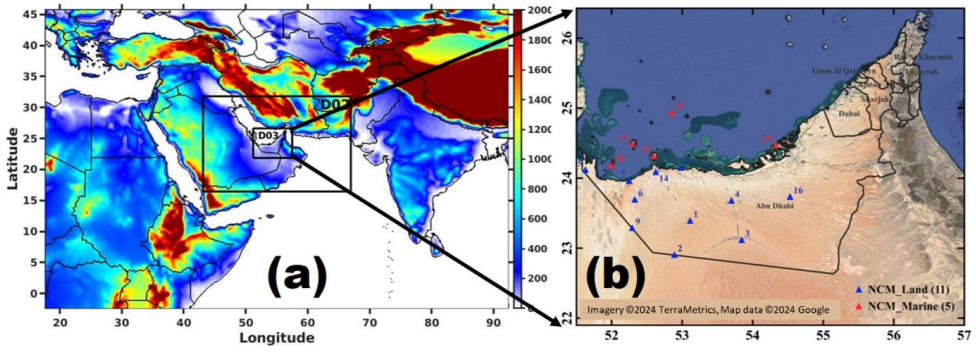

Figure 1: Model Configuration: (a) The WRF domain configuration consists of three telescoping nests, with the outermost boundaries denoting the parent grid (D01). D02 and D03 are the nested domains. Right panel (b) is a zoom of the innermost domain (D03) showing the spatial distribution of the 16 meteorological stations (land stations are denoted by blue triangles, and marine stations are represented by red triangles). The shading in (a) represents the orography (m). Further details about the stations are given in Tables 2.

Table 1: WRF-chem model setup

Model set-up	**Option**
Model version	4.3.1
Domain	3 domains
Horizontal resolution	D01:27km, D02:9km and D03:3km
Simulation period	Monthly runs from June 2018 and December 2018
Model spin-up period	2 days in each month
Vertical resolution	45 eta levels up to 50 hPa.
Domain size	D01: 283×205 grids, D02: 271×193 grids and D03: 256×178 grids
Meteorological boundary	NCEP FNL reanalysis (0.25°, 6-hourly)
Chemical boundary	CAM-Chem (Emmons, Fasullo, et al., 2020)
Physical Process	**Parameterization Scheme**
Microphysics	Morrison double moment (Morrison et al., 2009)
Cumulus parameterization	Kain-Fritsch (Kain, J.S, 2004)
Shortwave radiation	Rapid Radiative Transfer Model for GCMs (RRTMG) (Iacono et al. 2008)

https://doi.org/10.5194/egusphere-2024-959
Preprint. Discussion started: 6 May 2024

Longwave radiation	Rapid Radiative Transfer Model for GCMs (RRTMG) (Iacono et al. 2008)
Land surface	Unified Noah land surface model (Tewari et al., 2004)
Planetary boundary layer	Yonsei University scheme (Hong, 2010)
Chemistry option	**Scheme used**
Gas phase chemistry	MOZART-4 (Emmons et al., 2010).
Aerosol chemistry	GOCART (Chin et al., 2002)
Photolysis	Madronich F-TUV (Madronich, 1987; Tie, 2003)
Biogenic emissions	MEGAN (Guenther et al. 2012)
Dry deposition	Wesely (Wesely 1989)

3. Data Sets and methodology

3.1 Meteorology observations

In this study, meteorological data from 16 automatic weather stations (AWS) operated by the National Center of Meteorology (NCM), UAE were utilized to assess the WRF-Chem simulations for air temperature at 2 meters above ground (T2m), wind speed at 10 meters (WS10m), and downward shortwave radiation flux at the surface (SR) during June and December of 2018. The spatial distribution of the stations across the UAE is illustrated in Fig. 1(b) (refer to Table 2 for details). These locations were categorically divided into two regions—land stations (station with ID number: 1-9,14 and 16) and marine stations (station with ID number: 10-13 and 15)—following the criteria outlined in Branch et al., (2021). Subsequent analyses are based on these two primary categories, with the land region comprising 11 stations (marked with green triangles) and the marine region comprising 5 stations (marked with yellow triangles) in Fig. 1(b). Additional information on the specifics, quality control measures, and other research studies based on NCM data can be found in the referenced literature (Branch et al., 2021; Fonseca et al., 2020, 2021, 2022; Temimi et al., 2020a).

Table 2 List of Automatic Weather Stations (AWS) utilized for evaluating the WRF-Chem model.

ID	Name	Lat.	Lon.	Altitude (m)	Region
1	Owtaid	23.40	53.11	160	Land
2	Mukhariz	22.91	52.89	130	Land
3	Mezaria	23.12	53.84	110	Land
4	Madinat Zayed	23.68	53.70	110	Land
5	Al Gheweifat	24.12	51.63	47	Land

https://doi.org/10.5194/egusphere-2024-959
Preprint. Discussion started: 6 May 2024

6	Bu Hamrah	23.51	54.53	136	Land
7	Barakah	23.96	52.25	5	Land
8	Al Qlaa	24.16	52.98	150	Land
9	Al Jazeera	23.29	52.29	70	Land
10	Yasat	24.19	52.00	115	Marine
11	Sri Bani Yas	24.32	52.60	101	Marine
12	Qarnen	24.94	52.85	26	Marine
13	Dalma	24.49	52.29	10	Marine
14	Al Ruwais	24.09	52.62	33	Land
15	Abu Dhabi	24.48	54.33	3	Marine
16	Al Tawiyen	25.56	56.07	186	Land

3.2 ERA-5 Reanalysis data

The fifth-generation European Centre for Medium-Range Weather Forecasts (ECMWF) reanalysis, known as ERA-5 (Hersbach et al., 2020), represents a significant advancement over its predecessor, the ERA-Interim reanalysis, introduced by Dee et al., (2011). ERA-5 incorporates a sophisticated four-dimensional variational (4D-Var) data assimilation method, utilizing the 41r2 cycle of the Integrated Forecast System (IFS). This system is enhanced by the integration of both a soil model and an ocean wave model, offering a comprehensive approach to climate data analysis. For the purposes of this research, we accessed ERA-5 data through the Copernicus Climate Change Service Climate Data Store (CDS). The dataset provides atmospheric observations across 137 hybrid vertical levels, with data available on the CDS interpolated onto 37 distinct pressure levels. These levels span from 1000 hPa, close to the Earth's surface, up to 1 hPa, reaching altitudes of approximately 80 km. Further details on the ERA-5 dataset are available in Dee et al., (2011) and Hersbach et al., (2020). Our study specifically utilized hourly data for a selection of meteorological parameters: air temperature at 2 meters above the ground (T2m), wind speed at 10 meters (WS10m), downward shortwave radiation flux at the surface (SR), and planetary boundary layer height (PBL), for the months of June and December 2018.

3.3 Satellite-borne observations

Launched by the European Space Agency (ESA) on October 13, 2017, the TROPOspheric Monitoring Instrument (TROPOMI) is aboard the Sentinel-5 Precursor (S5P) satellite, operating in a near-polar sun-synchronous orbit. Positioned at an altitude of 817 km, the S5P satellite crosses the equator at a local solar time of 13:30, boasting a wide swath of

https://doi.org/10.5194/egusphere-2024-959
Preprint. Discussion started: 6 May 2024

approximately 2600 km, and providing daily global coverage. TROPOMI features four distinct spectrometers that measure the ultraviolet (UV) and UV-visible (UV-VIS) range (270 to 500 nm), near-infrared (NIR) range (675 to 775 nm), and short-wave infrared (SWIR) range (2305 to 2385 nm) spectral bands (Veefkind et al., 2012). Notably, the last two spectral bands, NIR and SWIR, are newly introduced in TROPOMI compared to its predecessor OMI (Ozone Monitoring Instrument). TROPOMI's data products encompass daily observations of trace gases, including CO, O_3, NO_2, CH_4, HCHO, aerosols, and cloud properties. The present study utilized daily NO_2, CO, and ozone column density level 2 products from TROPOMI, downloaded from the GES DISC website (https://disc.gsfc.nasa.gov/) for the period of June 1-30 and December 1-31, 2018. The specific data sets employed for the present study includes S5P_OFFL_L2__O_3 for O_3, S5P_OFFL_L2__CO for CO, and S5P_OFFL_L2__NO_2 for NO_2, covering the study region bounded by longitudes [51°,58°] and latitudes [21°, 27°]. Further details regarding each product, retrieval algorithm, and validation results are summarized in the subsequent section.

TROPOMI retrieval of NO_2 columns are derived using UV-VIS spectrometer backscattered solar radiation measurements in the wavelength range of 405-465 nm and provides total and tropospheric NO_2 vertical column density with a near-nadir resolution of 7x3.5 km. The total NO_2 slant column density (SCD) is retrieved from the measured solar irradiance spectra using the Differential Optical Absorption Spectroscopy (DOAS) method. Tropospheric and stratospheric slant column densities are separated from SCD by a data assimilation system based on the chemistry transport model V5 (TM5-MP). Afterwards, they are converted to vertical column densities (VCDs) with the help of look-up table of altitude-dependent air-mass factors (AMFs) and information on the vertical distribution of NO_2 from TM5-MP apriori profile with a horizontal resolution of 1^o x 1^o and a time step of 30 min (Boersma et al., 2018; Van Geffen et al., 2022). The TROPOMI NO_2 product has been extensively evaluated using ground-based and aircraft observations and found to have a high correlation and low bias of less than 30% with respect to in-situ measurements (Griffin et al., 2019; Ialongo et al., 2020). We used the reprocessed (RPRO) TROPOMI NO_2 data files with processor version of 1.2.2, for the study period. Additionally, two more NO_2 products are available such as offline (OFFL) and near-real time (NRTI). NRTI data files are generated using TM5-MP forecast data rather than analysis data as with REPO and OFFL files (Van Geffen et al., 2022). The differences between the OFFL/REPO and NRTI NO_2 products are generally very small (references therein Ialongo et al., 2020).

https://doi.org/10.5194/egusphere-2024-959
Preprint. Discussion started: 6 May 2024

The Shortwave Infrared Carbon Monoxide Retrieval (SICOR) algorithm is used to retrieve CO column densities from TROPOMI in the spectral range of 2305 to 2385 nm (Landgraf et al., 2016). The SICOR algorithm accounts for a profile-scaling approach that scales retrieved CO total column to the a priori reference profile. The a priori reference profiles are taken from the global chemistry transport model simulations of TM5-MP, and they vary based on the location, month and year (Krol et al., 2005). The detailed outline of all settings and other auxiliary data sets used for CO retrievals are outlined in the Landgraf et al., (2016). This study limits the analysis to CO pixels corresponding to clear-sky conditions and mid-level clouds by filtering the data using the quality flag variable (qa_value). The scenes corresponding to qa_value > 0.5 are used in this current analysis as suggested in the ATBD (algorithm theoretical baseline document; Landgraf et al., 2016). In this present work, TROPOMI CO measurements for the period from 1-30 June and 1-31 December, 2018 have been analysed. Moreover, we use either the reprocessed (RPRO) or offline (OFFL) data files from most recent processor versions depending on availability for a given day of observations. Wizenberg et al., (2021) compared global TROPOMI retrieved CO total columns with corresponding ACE-FTS (Atmospheric Chemistry Experiment- Fourier transform spectrometer) columns for the period from November 2017 to May 2020 and found a small relative bias of -0.83% with a correlation coefficient of 0.93 between two data sets. Similar results were also found between TROPOMI CO with corresponding CO fields from the ECMWF assimilation system: Borsdorff et al. (2018) reported a small mean difference between the two data sets of 3.2% with a correlation coefficient of 0.97.

TROPOMI also provides total ozone column (TOC) and ozone profile data at 15 pressure levels. It measures radiances and irradiances in the ultraviolet wavelength of 270-330 nm and provides the ozone profile information. The Optimal Estimation (OE) algorithm is used to retrieve the ozone profile data. Before this stage, various pre-processing steps are applied to the measured spectra before the estimation of the ozone profile. The main process of the algorithm is the OE method, which combines the information from the measured spectra with the a-priori information. The a-priori information is based on climatology as described in the Labow et al., (2015). The description of the various pre-processing steps performed to retrieve ozone profiles is presented in the Algorithm Theoretical Basis Document (Veefkind, et al., 2021). The validation of TROPOMI retrieved ozone profile data against the ground-based

https://doi.org/10.5194/egusphere-2024-959
Preprint. Discussion started: 6 May 2024

measurements reported a median bias of 0.3% for OFFL/REPO products while 0.8 % for NRTI ozone products (Lambert et al., 2023).

3.4 Satellite data processing

In order to quantitatively compare the WRF-chem simulations with satellite measurements, the model outputs must be processed using the appropriate method as described in the literature (Kumar et al., 2012). Direct comparison between satellite retrievals and model outputs is not recommended as satellite measurements depend on column averaging kernels (AK) and a-priori profiles. The AK vector, representing the vertical sensitivity of the retrieved column to the partial column at different vertical levels, should be employed to convolve the model simulations.

The column density from the WRF-Chem model is re-gridded to match the TROPOMI instrument's grids and is vertically interpolated to the TROPOMI pressure levels before it is multiplied by the AK. This treatment of the WRF-Chem-simulated profile with the column averaging kernels allows for a comparison that is independent of the chemical transport model (CTM) a-priori assumptions and the vertical sensitivity of the retrieval process; therefore, it can be directly compared with the TROPOMI-derived tropospheric column of NO_2. The TROPOMI-NO_2 products also provide a column averaging kernel matrix. In the case of TROPOMI-NO_2, the application of the column AK averaging kernel accounts for the vertical distribution and sensitivity of the measurements, as classically done by Borsdorff et al., (2014) as:

$$X_{ret} = X_{a\ prior} + AK \times (X_{true} - X_{a\ prior}) + e_x \quad \text{----------(1)}$$

where, X_{true} is model simulation profile of trace gas; X_{ret} is the retrieved profile or smoothed model profile; e_x represents the error on the retrieved trace gas profile; $X_{a\ prior}$ is the a-priori information provided in the TROPOMI data set. For TROPOMI-NO_2 data, the contribution of the a priori profile and error on the retrieved profile can be eliminated, as explained in Borsdorff et al., (2014). The eq. (1) simplifies to

$$X_{ret} = AK \times (X_{true}) \quad \text{---------- (2)}$$

For validation of ozone and CO total column, we have used the TROPOMI ozone and CO profile level 2 data product S5P_OFFL_L2__O_3__ and S5P_OFFL_L2__CO__ that provides the ozone and CO concentrations at 15 and 50 pressure levels, respectively. This data product

https://doi.org/10.5194/egusphere-2024-959
Preprint. Discussion started: 6 May 2024

also includes the a priori information and column averaging kernel for each pressure level. In order to compare our model profile with this dataset, the model output is horizontally and vertically interpolated to TROPOMI grids and vertical levels. The final model profile was calculated by the Eq. (3)

$X_{ret} = X_{a\,prior} + AK \times (X_{true} - X_{a\,prior})$ ----------(3)

Since the highest vertical level in WRF-Chem-simulated trace gas concentration is 50 hPa, the remaining vertical layers of ozone and CO were made equal to the a priori concentration of respective trace gases as described by ATBD (Landgraf et al., 2016).

3.5 Evaluation methodology

Meteorological parameters from the WRF-Chem model were extracted for the grid points closest to the surface observation sites of NCM. Meteorological parameters were categorized and averaged for land and marine regions for the regional analysis. Consequently, further analyses based on these categories are presented in subsequent sections of the article. To enable comparison of atmospheric column data from the TOPOMI satellite retrievals with WRF-Chem outputs, the data must undergo smoothing through an appropriate method described in Section 3.4, as direct comparison between satellite retrievals and simulations is not feasible due to discrepancies highlighted in previous literature. Additionally, owing to the spatial resolution differences between WRF-Chem and ERA5 datasets, it is necessary to remap the model data to the ERA5 grids for accurate comparison. A wide range of statistical parameters is available for evaluating model simulations. In this study, we employed statistical skill scores including the Pearson correlation coefficient (r), the Mean Bias (MB), the Root Mean Square Error (RMSE), and the Mean Absolute Error (MAE), which have been extensively discussed and applied in similar contexts (Fonseca et al., 2021; Ivatt & Evans, 2020; Temimi et al., 2020b).

The following equations (eq. 4 to eq. 7) are used to calculate these statistical matrixes in the present study,

$$r = \frac{\sum_{i=1}^{N}[(O_i-\overline{O_i})(M_i-\overline{M_i})]}{\sum_{i=1}^{N}(O_i-\overline{O_i})^2 \sum_{i=1}^{N}(M_i-\overline{M_i})^2}$$ ----------(4)

$$\text{RMSE} = \left(\frac{1}{N}\sum_{i=1}^{N}(M_i - O_i)^2\right)^{\frac{1}{2}}$$ ----------(5)

$$\text{MB} = \frac{1}{N}\sum_{i=1}^{N}(M_i - O_i)$$ ----------(6)

https://doi.org/10.5194/egusphere-2024-959
Preprint. Discussion started: 6 May 2024

$$\mathrm{MAE} = \frac{1}{N}\sum_{i=1}^{N}|M_i - O_i| \quad \text{----------(7)}$$

where O_i denotes the i-th observation, M_i represents the corresponding WRF-chem simulated value, and N is the number of model and observation pairs. $\overline{M_i}$ and $\overline{O_i}$ are the model and observational means (i.e. average of 1-30, June and 1-31 December), respectively. The correlation coefficient (r) is an indication of the phase agreement between the modelled and observed time-series. The RMSE measures the average error in the model, and the MAE determines the mean error between the model and observations regardless of whether it is an under or overestimate. The MB is a measure of the systematic error and gives information whether the model is over or underpredicting the corresponding observed values.

4. Results and Discussion

4.1 Model performance for meteorological variables

The general ability of the WRF-Chem model to reproduce realistic spatio-temporal patterns of the most relevant physical and chemical variables is assessed by comparing the simulated output with the observational data for June and December for the year 2018, reflecting the contrasting summer and winter conditions over the UAE. Determining the accuracy of WRF-Chem simulations by validating meteorological conditions in the study area is crucial before utilizing the model's output for air quality applications. In this regard, we have conducted a comparison of the model's T2m, WS10m, and SR outputs with measurements from observational data sets. Additionally, we have compared the boundary layer height from the model with the ERA5 reanalysis product. These parameters were chosen due to their significance in influencing most air pollutants (Ritter et al., 2013). Notably, the ERA5 reanalysis data boasts a high spatial resolution of approximately 28 km, making it superior to other reanalysis datasets in this aspect. Our comparison involved analysing the hourly results from both ERA5 and ground-based datasets against WRF-Chem for two distinct months in 2018. Detailed results of this comparison are presented below.

4.1.1 Evaluation against surface-based observations

The WRF-Chem model effectively represented the observed variations in T2m, WS10m, and SR across all 16 meteorological stations during June and December 2018. The WRF-Chem model generally underestimated T2m values by less than 0.5 °C in June and overestimated them in December by less than 1.3 °C across the majority of locations. Correlation coefficients

https://doi.org/10.5194/egusphere-2024-959
Preprint. Discussion started: 6 May 2024

for the observed T2m with model simulations were between 0.66 to 0.99 in June, slightly increasing to a range of 0.70 to 0.99 in December. The MB for T2m varied from -0.04 to +1.19 °C in June and -2.17 to +0.50 °C in December, with the RMSE spanning from 0.8 to 5.9 °C in June and 0.9 to 4.1 °C in December. Conversely, the outcomes for WS10m and SR demonstrated variability across different stations. The model performance demonstrates significant enhancements over previous research conducted in this region. For instance, Fonseca et al., (2020) observed a warm bias of 1-3 °C in WRF simulations across the UAE for both winter and summer seasons. This observation aligns with similar findings reported by Schwitalla et al., (2020) and Wehbe et al., (2017). The enhanced performance of the model may be attributed to the present model configuration which differs from that used in previous studies.

We concentrate on evaluating the model's performance at a regional scale, as delineated by land (encompassing 11 sites) and marine stations (comprising 5 sites), detailed in section 3.1.1. Table 3 presents an extensive evaluation of the statistical verification scores for essential meteorological variables at these categories within the UAE. In the month of June, the model slightly underestimated the T2m values in both land and marine settings, with a underestimation of 0.37 °C and 0.48 °C, respectively, despite an overprediction of SR. This arises because of colder temperatures in particular in the evening and night-time hours, a bias highlighted by other studies such as Temimi et al. (2020b) and Branch et al. (2021). This has been attributed to deficiencies in the model's physics and/or dynamics, in particular in the land surface model and surface properties, a cold bias in the forcing dataset, and an incorrect representation of the concentration of aerosols and greenhouse gases. Despite this, the model achieves notable correlation coefficients (r) of 0.91 for land regions and 0.83 for marine regions. The lower correlation observed in marine regions possibly arises from the more muted diurnal cycle (Fig. 2) and the model's inability to properly represent the complex land-sea mask even at 3 km spatial resolution. Similar results were reported in Abida et al., (2022), where the WRF model demonstrates improved accuracy in inland areas compared to offshore or coastal regions. The RMSE (MAE) values stand at 3.57 °C (2.68 °C) for land and 1.67 °C (1.47 °C) for marine regions, respectively. In December, the T2m predictions by the model show an overestimation, marked by 0.76 °C in land and 1.30 °C in marine regions. The model maintains strong correlations, with r = 0.92 for land and r = 0.90 for marine regions, underscoring its consistent performance. The RMSE (MAE) values recorded are 2.87 °C (1.66 °C) for land and 2.57 °C (1.37 °C) for marine regions, illustrating the model's accuracy in capturing temperature

https://doi.org/10.5194/egusphere-2024-959
Preprint. Discussion started: 6 May 2024

fluctuations over these regions. For WS10m, the model effectively aligns with observed values, showing good agreement in both land and marine settings. In June, it slightly overestimated the wind speed in the marine region by 0.51 m/s, a trend that is also reflected in the RMSE metrics, which are marginally higher for marine areas compared to land (0.08 m/s). In December, it notably overestimated wind speeds in marine regions by 0.92 m/s, while the overestimation was slightly less in land areas, at 0.38 m/s. Despite this, the correlations remain robust in both seasons, highlighting the model reliability in capturing wind speed variations across different environments. The model representation of SR demonstrates a similar pattern of accuracy and overestimation. In June, the model tends to overestimate SR across both regions, which has been reported in Fonseca et al. (2020) and Temimi et al. (2020b), yet it achieves a more accurate depiction in December. A possible explanation is a reduced aerosol loading in the model, with the summer featuring higher atmospheric aerosol amounts than the winter season (Nelli et al., 2021), with WRF also exhibiting a tendency to underpredict the observed cloud cover in the region. Although the correlations for SR are slightly lower, especially in the marine regions, they still indicate a reasonable level of model performance. Overall, the model tends to overestimate WS10m and SR across both seasons, while it underestimates the T2m in winter and overestimates it in summer. Such variable performance of the model has been noted in findings from prior research (for example, Schwitalla et al., 2020; Wehba et al., 2017; Fonseca et al., 2020; Abida et al., 2022). Furthermore, a more detailed analysis of the biases identified in T2m and WS10m, including an examination of the diurnal variation of these parameters, is presented in the following sections.

Table 3: Statistical verification scores for evaluation against weather station data: skill scores for air temperature at 2m (T2m), wind speed at 10m (WS10m) and downward shortwave radiation flux (SR) for 16 meteorological stations (categorised into land and marine regions) over the United Arab Emirates (UAE).

Parameter	**Month**	**Region**	**MOD**	**OBS**	**MB**	**MAE**	**R**	**RMSE**
T2m (^{o}C)	June	Land	35.70	36.07	-0.37	2.68	0.91	3.57
		Marine	33.54	34.03	-0.48	1.47	0.83	1.67
	Dec	Land	21.84	21.08	0.76	1.66	0.92	2.87
		Marine	24.02	22.72	1.30	1.37	0.90	2.57
WS10m (m/s)	June	Land	4.24	4.16	0.08	0.90	0.88	1.35
		Marine	4.44	3.92	0.51	1.01	0.78	1.09
	Dec	Land	3.29	2.91	0.38	0.63	0.88	0.95

https://doi.org/10.5194/egusphere-2024-959
Preprint. Discussion started: 6 May 2024

		Marine	4.26	3.35	0.92	1.12	0.89	1.54
SR (W/m^2)	June	Land	352.0	279.7	72.4	197.1	0.87	327.1
		Marine	349.3	264.9	84.4	273.4	0.68	358.7
	Dec	Land	192.7	177.2	15.5	124.3	0.85	231.2
		Marine	183.8	171.7	12.1	188.8	0.59	240.7

Figure 2, (a) and (b), presents a comparative analysis of the average diurnal variation in T2m from WRF-Chem simulations and observations at both land and marine sites investigated in this study, for the summer and winter seasons of 2018, respectively. The observed and modelled T2m data exhibit a close alignment over land and marine locations, although some discrepancies are evident. During the daytime, there is a tendency for the model to exhibit a warm bias, while at night and evening, a cold bias is more apparent. Such discrepancies in temperature have been reported before (Abida et al., 2022; Branch et al., 2021; Fonseca et al., 2021; Schwitalla et al., 2020; Temimi et al., 2020a). Overall, the WRF-Chem model displays a consistent cold bias of less than 0.5 °C for both environments during the summer months. In contrast, during winter, the model shows a warm bias ranging from 0.8 to 1.3 °C. This is in contrast to findings by Branch et al. (2021), which indicated an increase in the nocturnal cold bias from winter to summer. Conversely, our study identifies a cold bias in the summer and a warm bias in the winter, persisting throughout the entire day over marine locations. The decrease in cold bias observed during summer in WRF-Chem simulations is a result of enhanced representations of updated surface and soil parameters over the study region.

https://doi.org/10.5194/egusphere-2024-959
Preprint. Discussion started: 6 May 2024

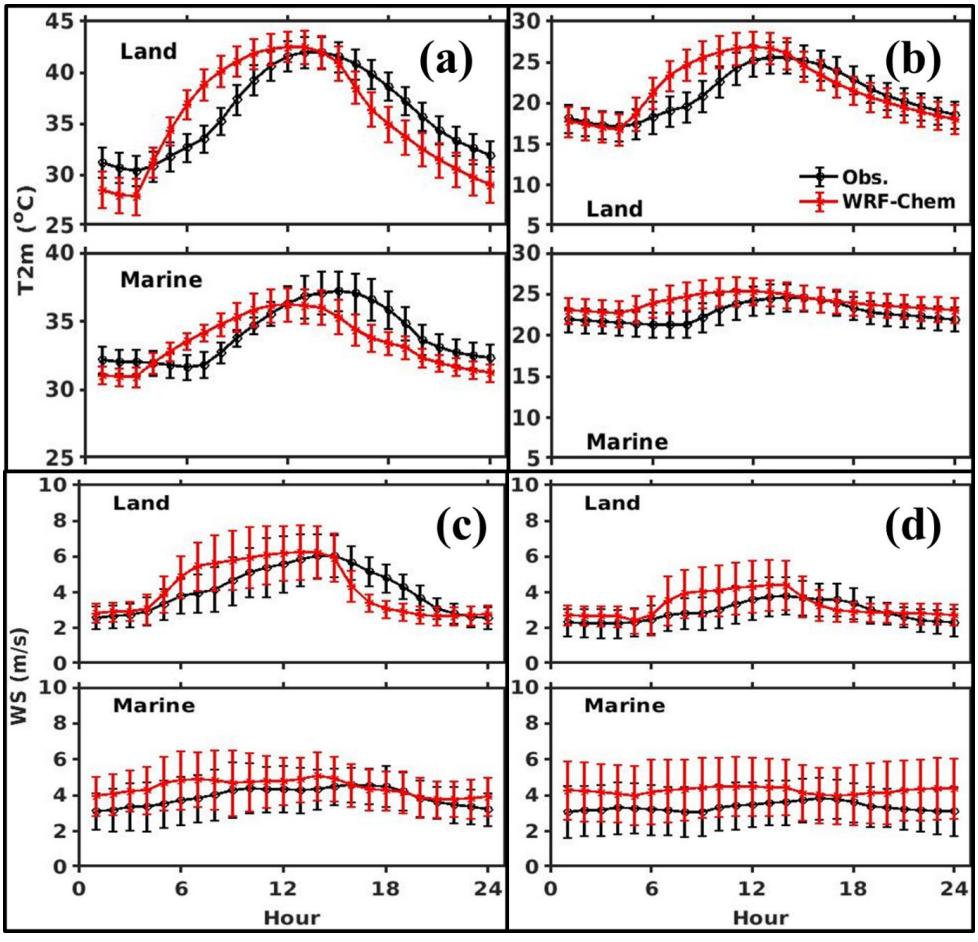

Figure 2: Air temperature and wind speed diurnal cycle: Diurnal cycles of spatial mean values of WRF-chem simulated (red) and observed (blue) air temperature at 2m (T2m; °C) in (a) (summer) and (b) (winter) for the regional categories of land and marine sites (c)-(d) are as (a)-(b) but for the wind speed at 10 m (WS10m; m/s). The averaged spatial standard deviation is represented by an error bar at each hour.

Figure 2, (c) and (d), showcase a comparative analysis of the mean diurnal variation in WS10m from model simulations and observations at both land and marine sites examined in this study, during the summer and winter of 2018, respectively. In both seasons, higher wind speeds are observed over marine sites, while lower wind speeds are found over land sites, reflecting sea and land circulations, respectively. It is indicated that wind speeds are higher during the daytime and lower during the night and evening hours. This pattern is especially pronounced over land sites compared to marine sites during both seasons. WRF-Chem tends to overestimate

https://doi.org/10.5194/egusphere-2024-959
Preprint. Discussion started: 6 May 2024

WS10m during both day and night, across all regions and seasons. Nonetheless, the model shows the smallest discrepancies over land, with biases being the least significant at 0.1 m/s during summer and 0.4 m/s in winter. In contrast, the biases over marine areas are more pronounced, at 0.5 m/s in the summer and 0.9 m/s in the winter. WRF-Chem tends to overestimate WS10m more significantly during winter, with less overestimation observed during summer. This discrepancy is linked to alterations in wind direction driven by land and sea breeze circulations. Consequently, numerous studies have previously emphasized the model's tendency for wind speed overprediction (Abida et al., 2022; Branch et al., 2021; Fonseca et al., 2021; Schwitalla et al., 2020; Temimi et al., 2020a**).**

4.1.2 Evaluation against ERA5 reanalysis data

In Fig. 3, a spatial comparison is presented between the averaged ERA5 T2m and the corresponding WRF-chem simulation output across the simulation domain during June and December of 2018. The model adeptly captures regional temperature variations, displaying underestimation in the southern regions and overestimation in the north-western region of the UAE. This observation suggests a comprehensive portrayal of temperature dynamics by the model, with specific tendencies in certain geographical areas. This observation is also supported by NCM data, for instance, at Mezaria (ID No: 3), which represents a southern land site, and at Abu Dhabi (ID No: 15), representing a northern marine site within the emirate of Abu Dhabi. The southern land site found an underestimation of 1°C, while the northern marine site exhibited an overprediction of T2m by WRF-chem. WRF-Chem overestimates the area-averaged temperature (T2m) over the UAE compared to ERA5 in both seasons. In contrast, NCM observations indicate an underestimation during the summer and an overestimation during the winter across the majority of sites. Kishta et al., (2023) reported that, minor discrepancies in temperature measurements between observational data and ERA5 reanalysis, identifying a strong correlation coefficient of 0.89 over Abu Dhabi. The spatial average of WRF-Chem and ERA5 values are 35.8 °C and 35.7 °C, respectively, with a small underestimation of 0.08°C over the UAE. The model displays a high correlation (r) of 0.97 and a RMSE of 2.3 °C, MAE of 2.2 °C in June. For December, the model showed a similar pattern, with a underestimation of 0.53 °C which is slightly higher as compared to June, r of 0.98, MAE of 1.0 °C and RMSE of 1.1 °C (Table 4).

Moreover, the analysis of the absolute differences between the two datasets highlighted the most pronounced discrepancies over the Arabian Gulf region, observable in both the summer and winter months. However, these discrepancies are notably more emphasised during the

https://doi.org/10.5194/egusphere-2024-959
Preprint. Discussion started: 6 May 2024

warmer months. WRF-simulated Sea Surface Temperatures (SSTs) are compared with both ERA5 and Group for High Resolution Sea Surface Temperature (GHRSST) data over the Arabian Gulf region (not shown). The comparison involved area-averaged daily values, considering that the diurnal amplitude of SST is 0.5 °K over this region as reported by Nesterov et al., (2021). The model showed an overestimation of 1.4 °K compared to both ERA5 and GHRSST during the summer. Similarly, in winter, its overestimated SSTs by 1.5 °K compared to ERA5 and by 1.3 °K compared to GHRSST. Furthermore, the model exhibited a significantly higher correlation in winter, achieving a correlation coefficient of 0.9 with both datasets. However, during the summer, it displayed variable correlations, with r=0.38 for ERA5 and r=0.20 for GHRSST. This observation suggests potential inaccuracies in the model simulation of temperature and wind speed in this region, which could be due to the sea surface temperature data utilized for model forcing. The temperature gradient plays a pivotal role in driving the land-sea breeze circulation. Higher temperatures observed over the Gulf could potentially weaken this circulation pattern, resulting in reduced transportation of cleaner marine air towards inland areas. Consequently, this reduction in the influx of marine air could obstruct the effective dispersion of pollutants across terrestrial regions, negatively impacting air quality and the spatial distribution of pollutants.

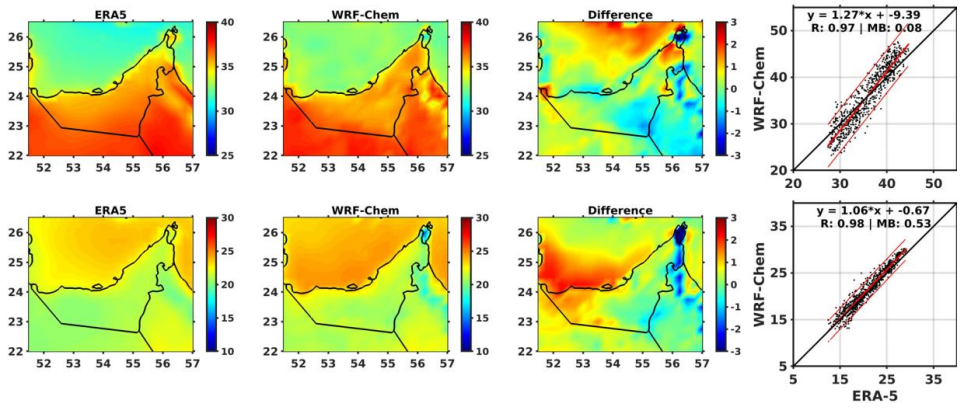

Figure 3: ERA-5 and WRF-Chem Air Temperature: Average 2-m air temperature (°C) obtained from ERA5 reanalysis (first panel), simulated by WRF-Chem (second panel), and the corresponding absolute differences (third panel) and scatter plots between the two datasets (fourth panel) during June (top) and December (bottom) 2018.

It is widely recognized that the Planetary boundary layer (PBL) plays a crucial role in the pollution transport process over the region. It constitutes the lowest part of the troposphere and is directly influenced by the Earth's surface. The PBL reaches higher elevations during summer,

https://doi.org/10.5194/egusphere-2024-959
Preprint. Discussion started: 6 May 2024

with its altitudes being lower in winter. There are noticeable differences in the PBL between land areas (approximately 2400–2500 m) and marine regions (about 1200–1500 m) (Basha et al., 2019). Basha et al. (2019) also discovered that ERA-Interim reanalysis data tend to underestimate PBL when compared with data obtained from Global Positioning System Radio Occultation (GPSRO) in most regions and in all the seasons. Chen et al., (2022) emphasized the critical role of the boundary layer in influencing air quality and facilitating the transboundary transport of pollutants. They noted that a higher boundary layer enhances the potential for pollutant transport to the Tibetan Plateau. Wang et al., (2022) highlighted the critical role of meteorological conditions in severe $PM_{2.5}$ pollution episodes. They noted that rapid cold air movement can quickly disperse pollutants, in contrast to the slow accumulation of pollutants under weak high-pressure systems. This slow build-up is characterized by low wind speeds, and low atmospheric boundary layer heights, which lead to prolonged heavy pollution periods.

In this study, we aim to compare the PBL as simulated by WRF-Chem with the ERA5 reanalysis, providing further specifics of model accuracy and performance. Fig. 4 shows a comparison of the mean ERA5 PBL with corresponding WRF-chem simulated values over the UAE for the months of June and December 2018. The absolute difference and scatter plot for these data sets are also shown. The spatial distribution of PBL across the UAE, as from ERA5 data, exhibits a consistent spatial pattern that aligns with the PBL simulated by WRF-Chem. There is a notable trend of increased PBL during the summer months and decreased PBL in the winter. This pattern generally corresponds with the seasonal temperature variations, where warmer summer temperatures contribute to an elevation in PBL, and cooler winter temperatures result in a reduction of PBL (Basha et al., 2019). In terms of PBL (averaged spatially for the UAE), the model exhibits good performance in capturing the regional variations. In June, the modelled PBL is at 669.8 m compared to 646.7 m in ERA5, with a correlation coefficient of 0.91 and a RMSE of 450.1 m. In December, the modelled PBL is 490.5 m compared to the ERA5 of 444.2 m, with a high correlation coefficient of 0.98 and an RMSE of 152.8 m (Table 4).

https://doi.org/10.5194/egusphere-2024-959
Preprint. Discussion started: 6 May 2024

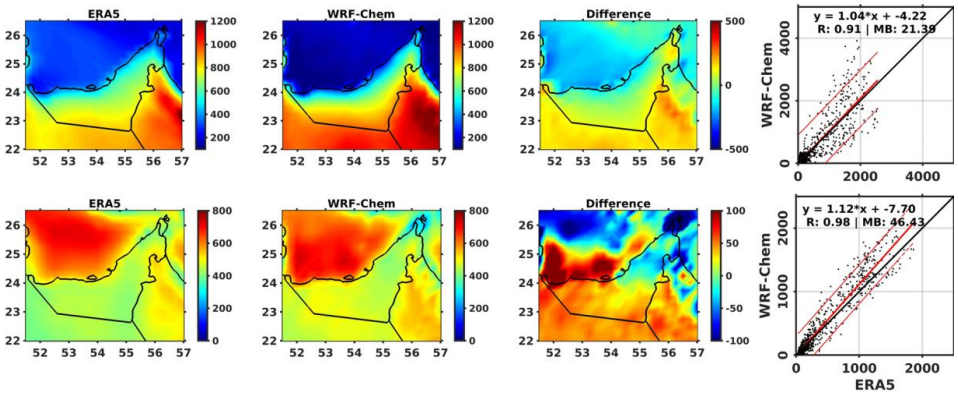

Figure 4: ERA-5 and WRF-Chem Boundary Layer Height: Same as Fig. 3, but for planetary boundary layer height (PBL).

In addition to T2m and PBL, Table 4 also summarizes the spatially averaged statistical verification scores for WS10m and SR over UAE. Regarding WS10m, it is accurately simulated by the model with small differences in MB (June: 0.08 m/s, Dec: 0.01 m/s), which are slightly larger compared to observations from land-based sites in Abu Dhabi and good correlations (June: 0.79, Dec: 0.80). The RMSE values are 1.7 m/s for June and 1.1 m/s for December. For SR, the model performs well, capturing the variability in radiation flux. In June, the modelled SR is 643.6 W/m² compared to the ERA5 of 576.5 W/m², with a high correlation of 0.99 and an RMSE of 75.3 W/m². Similarly, in December, the modelled SR is 460.8 W/m² compared to the ERA5 of 438.1 W/m², with a correlation of 0.97 and an RMSE of 76.1 W/m². Overall, these results indicate a very good performance of the WRF-chem model in simulating meteorological parameters over the UAE during the specified months. This rigorous evaluation of meteorological parameters showed that WRF-Chem's simulated values closely align with both ground-based and reanalysis datasets. Since WRF-Chem simulates meteorology and chemistry simultaneously, accurate meteorological simulations are crucial for the precise computation of chemistry within the model domain.

Table 4: Statistical verification scores for evaluation against ERA-5 data: skill scores calculated for model simulations for air temperature at 2m (T2m), wind speed at 10m (WS10m), downward shortwave radiation flux (SR) and planetary boundary layer (PBL) during June and December of 2018 over the United Arab Emirates.

https://doi.org/10.5194/egusphere-2024-959
Preprint. Discussion started: 6 May 2024

Parameter	Month	MOD	ERA5	MB	MAE	R	RMSE
T2m (^{o}C)	June	35.82	35.73	0.08	2.17	0.97	2.28
	Dec	21.61	21.08	0.53	0.99	0.98	1.12
WS10m		4.34	4.26	0.08	1.26	0.79	1.7
(m/s)		3.05	3.07	0.01	0.87	0.8	1.1
SR (W/m^2)		643.6	576.5	67.1	85	0.99	75.3
		460.8	438.1	22.8	69.5	0.97	76.1
PBL (m)		669.8	646.7	21.4	271.6	0.91	450.1
		490.5	444.2	46.4	113.8	0.98	152.8

4.2 Model performance with respect to gaseous pollutants

The study incorporates comparative assessments with satellite data from the TROPOMI instrument. This includes evaluations of the tropospheric column of NO_2 (denoted as TROPOMI-NO_2), total column CO (TROPOMI-CO), and total column ozone (TROPOMI-O_3) for the corresponding periods within the UAE. Detailed outcomes of these comprehensive assessments are discussed in the following subsections. The WRF-Chem model exhibited commendable proficiency in replicating the satellite-derived measurements of these pollutants throughout the UAE over the summer and winter seasons of 2018. The satellite overpass takes place daily at 13:30 local time; therefore, model simulations corresponding to this time are utilized here for comparison over the study area. After smoothing the model concentrations using the a priori and averaging kernel matrix as detailed in Section 3.4, the results were compared with the corresponding TROPOMI products.

In the troposphere, oxides of nitrogen (NOx=NO+NO2) are crucial for the mechanisms of ozone production and depletion in the presence of sunlight. Due to their shorter lifespan, their concentrations are primarily linked to emission sources. As a result, NOx is more susceptible to inaccuracies in emission estimates compared to other criteria pollutants. The Environment Agency – Abu Dhabi (2018) reported that oil and gas, road transport, and electricity generation are the primary sectors contributing to NOx total emissions, accounting for 42%, 34%, and 13% respectively, for the base year of 2015 in the Emirate of Abu Dhabi. In Fig. 5, the average spatial distributions of both model-simulated and TROPOMI-retrieved tropospheric column NO_2 are presented. Additionally, the spatial discrepancies between simulated and retrieved

https://doi.org/10.5194/egusphere-2024-959
Preprint. Discussion started: 6 May 2024

columns are illustrated by absolute differences (see third row) and scatter plots between the two datasets are depicted (see fourth row) for June (left) and December (right) 2018 across the study region. The satellite retrievals indicated elevated levels of NO_2 column, exceeding $12x10^{15}$ molecules/cm^2, in densely populated and industrial areas and the adjacent regions of Dubai and Abu Dhabi in both summer and winter. Conversely, lower NO_2 values, less than $5x10^{15}$ molecules/cm^2, were observed over the less urbanized areas. The higher columns are associated with significant economic development driven by a high demand in power generation and water desalination projects, which primarily depends on the combustion of fossil fuels in big cities like Dubai and Abu Dhabi (Abuelgasim & Farahat, 2020; Li et al., 2010). The model effectively reproduced the spatial distributions of NO_2 during summer and winter of 2018 as depicted in Fig. 5. Although, the model overestimation is close to zero in rural areas, it can be as high as 10^{16} molecules/cm^2 in areas of high pollution, specifically over Dubai and Abu Dhabi. Conversely, it underestimates up to 10^{16} molecules/cm^2 in the Ras Al Khaimah emirate; the sixth-largest city by population and home to the global ceramic manufacturing company, RAK Ceramics. This observation is not unexpected, as urban and industrial areas frequently report elevated pollutant emissions stemming from urban activities, which are significantly high and present challenges that models often struggle to accurately capture these changes. This discrepancy also suggests that anthropogenic and industrial emissions might be improperly represented in the EDGAR emission inventory. Challenges range from the incomplete characterization of emissions in source regions to the impact of model resolution on capturing sub-grid emission sources. Additionally, Hoshyaripour et al., (2016) found that the PBL is shallower and more stable at night when simulated with the YSU boundary layer scheme, resulting in a higher accumulation of NOx in the surface layers. Such insights were constrained in the present model evaluation, which is primarily focusing on temporal variability of gaseous pollutants on a daily basis, and did not encompass diurnal variations. Incorporating these diurnal variations in future model simulations over this region may enhance the assessment's accuracy. Additionally, the existing model configuration does not include the formation of secondary aerosols in its simulations, indicating a potential area for improvement in future versions. Additionally, the absence of vertical distribution of anthropogenic emissions in the model simulations also plays a pivotal role in these model discrepancies. The satellite retrieved TROPOMI-NO_2 averaged for the UAE is 0.21 x 10^{16} molecules/cm^2 in summer and 0.24 x 10^{16} molecules/cm^2 in winter. The corresponding model simulated column is 0.46 x 10^{16} and 0.43 x 10^{16} molecules/cm^2 respectively. The model demonstrated a strong correlation with satellite NO_2 column measurements, achieving

https://doi.org/10.5194/egusphere-2024-959
Preprint. Discussion started: 6 May 2024

correlation coefficients of 0.95 for summer and 0.94 for winter (refer to Table 5). It showed a slight tendency to overestimate NO_2 levels more in summer, with a discrepancy of 0.24 x 10^{15}, compared to 0.19 x 10^{15} molecules/cm^2 in winter. Moreover, the evaluation shows RMSE values of 0.1 x 10^{15} to 0.12 x 10^{15} molecules/cm^2 and MAE values of 0.20 to 0.25 x 10^{15} molecules/cm^2 during the seasons.

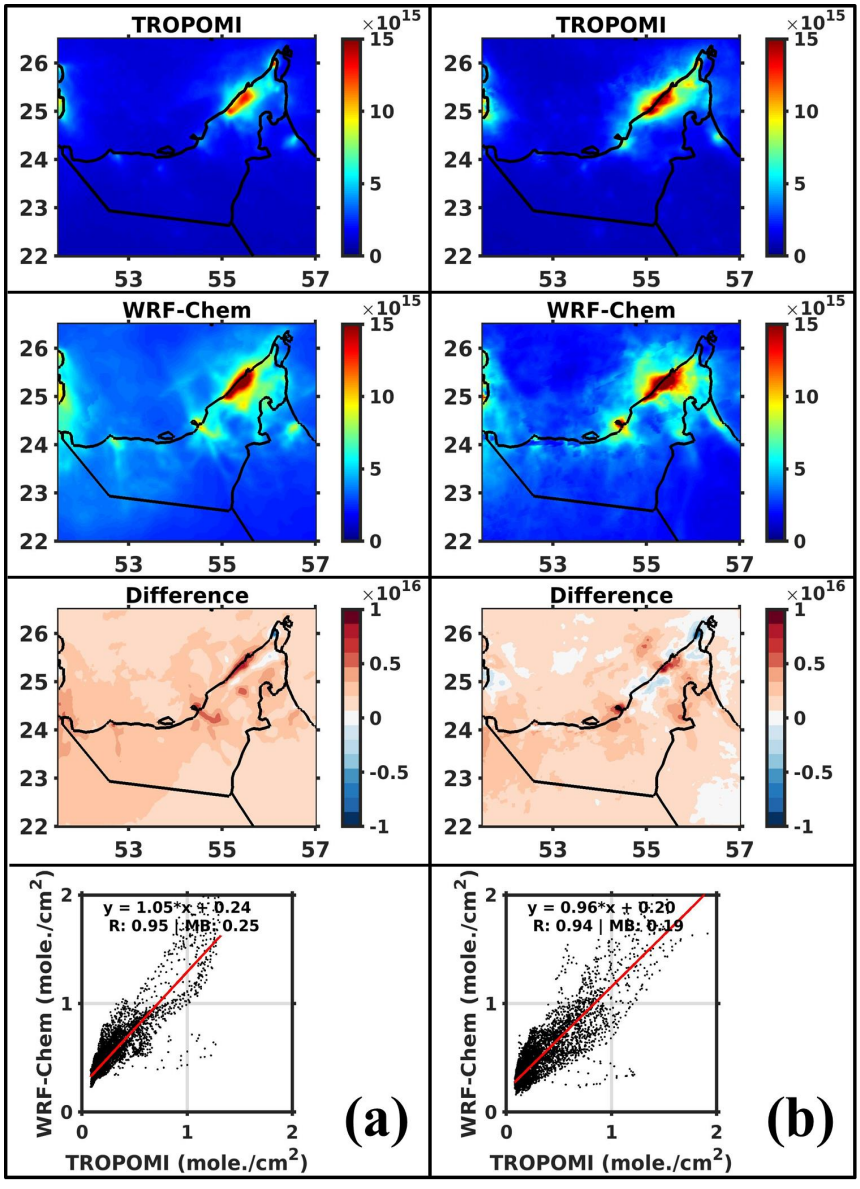

https://doi.org/10.5194/egusphere-2024-959
Preprint. Discussion started: 6 May 2024

Figure 5: Evaluation of WRF-chem against satellite-derived NO_2: average spatial pattern of tropospheric column NO_2 (mole. /cm^2) obtained from TROPOMI satellite (1st row), simulated by WRF-Chem (2nd row), corresponding absolute difference (model minus TROPOMI) (3rd row) and scatter plots between two daily data sets (4th row) during (a) June and (b) December in 2018.

In Fig. 6, the average spatial distributions of both model-simulated and TROPOMI-retrieved total CO column are presented. Also, the absolute difference of WRF-Chem simulations with TROPOMI-CO is depicted along with scatter plots between them during summer and winter of 2018 over UAE. The statistical metrics comparing these datasets are provided in Table 5. The TROPOMI-retrieved CO columns display values of 1.87 and 1.89 x 10^{18} molecules/cm^2 for summer and winter, respectively. In contrast, the simulated columns show values of 2.35 for summer and 0.76 x 10^{18} molecules/cm^2 for winter. Thus, comparing WRF-Chem and TROPOMI-CO data reveals more pronounced discrepancies, with a minor overestimation of 0.48 x 10^{18} molecules/cm^2 in summer and a significant underestimation of 1.13 x 10^{18} molecules/cm^2 in winter. Shami et al., (2022) discovered that the EDGAR emissions inventory underestimates CO emissions when compared to Lebanon's national emission inventory, identifying the road transport sector as the primary source of CO emissions. Consequently, EDGAR's estimates for CO emissions are lower than those provided by Waked et al., (2012) for the same region. The Environment Agency – Abu Dhabi (2018) reported that the road transport sector is the primary source of CO emissions in Abu Dhabi, accounting for 74% of the total CO emissions. Additionally, the industrial sector contributes 21% to the total CO emissions. Kumar et al. (2022) observed an underestimation of CO by the WRF-Chem model, attributing it to an inaccurate representation of anthropogenic emissions on the vertical scale. This could result in a more rapid deposition of CO molecules at the surface, thereby leading to the observed underestimation.

The model output correlates reasonably well with TROPOMI-CO with r of 0.71 and 0.86 while RMSE of 0.04 to 0.02 x 10^{18} molecules/cm^2 in summer and winter respectively (Table 5). In both seasons, the lower correlation coefficients for TROPOMI-CO as compared to TROPOMI-NO_2 suggest a less robust linear relationship between the TROPOMI and WRF-chem CO levels. This variation in performance might be attributed to the complexities inherent in modelling and observing CO distributions, which can be influenced by local emission sources, atmospheric chemistry, and transport processes. These findings are consistent with research conducted in India, where Dekker et al. (2019) reported a correlation of 0.81 between TROPOMI and WRF-Chem CO levels during a high pollution episode during November 2017.

https://doi.org/10.5194/egusphere-2024-959
Preprint. Discussion started: 6 May 2024

Similarly, in East Asia, Zhang et al. (2016a) documented correlations between WRF-Chem simulated and MOPITT retrieved CO columns, with r of 0.59 and RMSE of 4.6 x 10^{17} molecules/cm^2 for summer, and 0.69 with RMSE of 5.2 x 10^{17} molecules/cm^2 for winter, respectively.

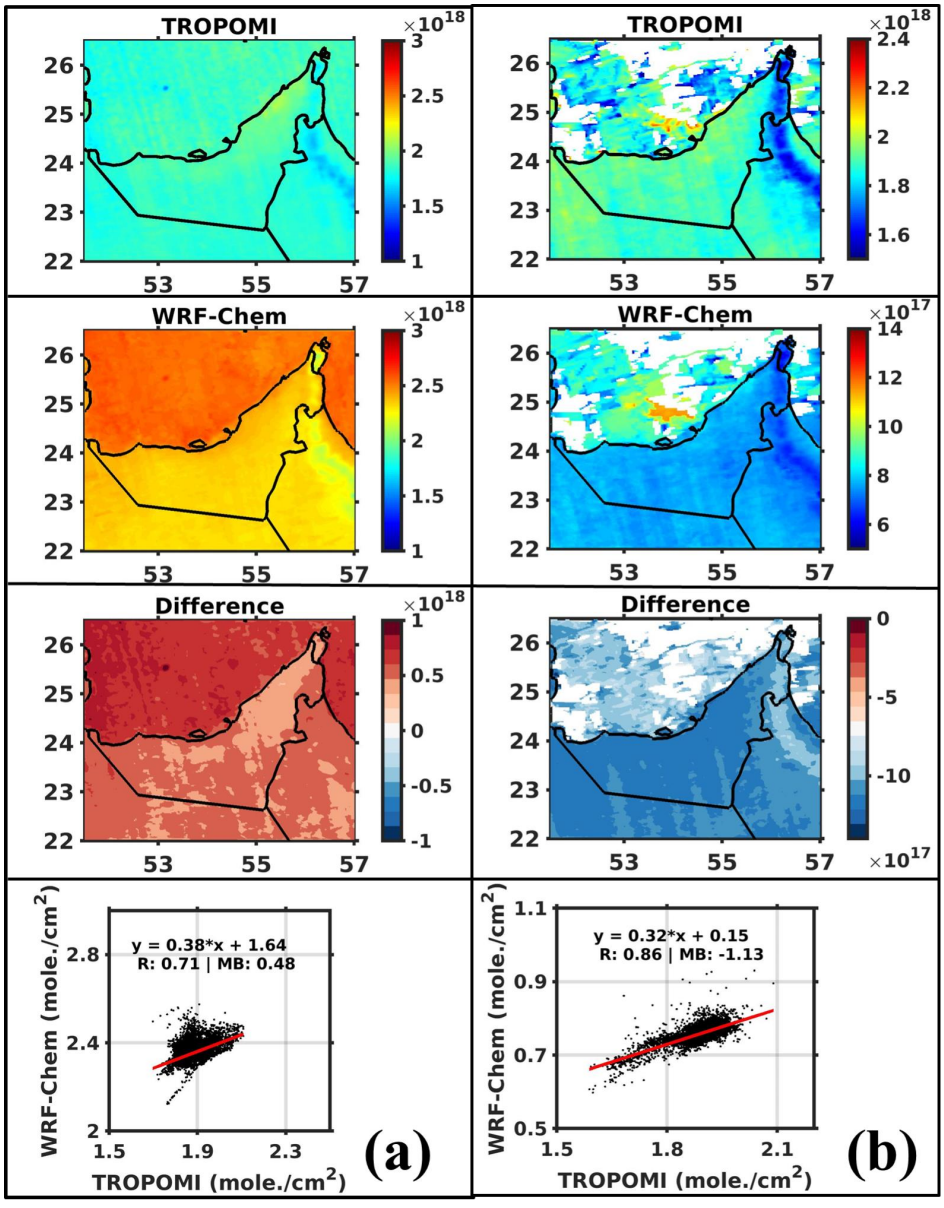

https://doi.org/10.5194/egusphere-2024-959
Preprint. Discussion started: 6 May 2024

Figure 6: Evaluation of WRF-Chem against satellite-derived CO: Same as Fig. 5 but for total column of CO

We also conducted a comparison of WRF-Chem simulated ozone levels with TROPOMI-retrieved total columns (TROPOMI-O_3), as illustrated in Fig. 7. This figure also presents both the absolute differences (3rd row) and scatter plots (4th row) between the two datasets for both seasons. The statistical comparisons between these datasets are detailed in Table 5. The TROPOMI-O_3 columns show higher values in summer, at 7.85 x 10^{18} molecules/cm^2, and lower values in winter, at 6.25 x 10^{18} molecules/cm^2. The WRF-Chem simulations closely match these variations, with values of 7.70 x 10^{18} molecules/cm^2 for summer and 6.06 x 10^{18} molecules/cm^2 for winter, respectively. Therefore, model output is strongly correlated to TROPOMI-O_3 columns with correlation of r=0.82 and 0.93 while RMSE (MAE) of 0.01(0.15 and 0.20 x 10^{18} molecules/cm^2) during summer and winter respectively. Many studies commonly report higher ozone concentrations in the summer and lower concentrations in the winter, a phenomenon primarily attributed to increased photochemical activity during the summer months (Reddy et al., 2012; Coates et al., 2016; Badia & Jorba 2015; Abdallah et al. 2018; Baldasano et al. 2011). The WRF-Chem model systematically underestimates ozone levels, with 0.15 and 0.20 x 10^{18} molecules/cm^2 both seasons respectively. Hu et al., (2021) highlighted that meteorological factors have a considerable effect on ozone production, noting from studies in China that temperature, relative humidity, and sunshine duration significantly influence ozone concentrations in descending order of importance. They also noted that strong solar radiation and elevated temperatures could enhance photochemical reactions, thereby increasing ozone formation. Zhang et al., (2020) pointed out that low wind speeds and high atmospheric pressure can impede the dispersion and dilution of pollutants, which in turn can lead to higher ozone accumulation. Lu et al., (2019) observed that high humidity conditions, with increased water vapor, could cause more significant chemical depletion of O_3, as water vapor interacts with excited ozone molecules to produce OH radicals. Hence, the meteorological conditions are conducive to ozone formation in the model but are insufficient to fully account for the model's significance underprediction of O_3. Sillman, (1999) demonstrated the ozone formation potential by its precursors being highly nonlinear rather than linear. Ozone formation can be either NOx-sensitive, meaning O_3 formation increases with an increase in NOx concentration, or VOC-sensitive, where O_3 formation increases with an increase in VOC concentration. However, Geng et al., (2007) observed that high NO_x concentrations in urban environments result in reduced OH radical levels, consequently

https://doi.org/10.5194/egusphere-2024-959
Preprint. Discussion started: 6 May 2024

decreasing ozone production, as loss of OH is evidenced by the chemical reaction NO2 + OH -> HNO_3. This observation is consistent with model simulations showing increased NO_2 levels but markedly lower ozone concentrations at an urban area in the UAE, illustrating the significant impact of NO_x on urban ozone formation. However, drawing such conclusions requires careful analysis of model simulations, suggesting that future work, particularly in the refinement of WRF-Chem evaluations, is essential. Future simulations should not only critically assess these findings but also aim to improve model fidelity by enhancing the representation of chemical processes and emissions. Adopting this approach will lead to more precise forecasts and a more profound grip of atmospheric chemistry, thereby enhancing air quality projections and fostering a more detailed understanding of pollution patterns over this region.

The disparities between WRF-Chem and TROPOMI data highlight the intrinsic challenges in air quality monitoring and prediction. WRF-Chem's limitations may stem from its dependency on emissions inventories, meteorological data, and the representation of atmospheric chemistry. TROPOMI, while offering high-resolution satellite observations, is subject to constraints related to retrieval algorithms and the influence of atmospheric conditions on measurement accuracy. Liu et al., (2022) identified that uncertainties in column observations stem from the challenges in differentiating between stratospheric and tropospheric contributions, as well as uncertainties in the tropospheric air mass factor and its spectral fitting. The integration of model predictions with satellite observations, alongside ground-based measurements, is crucial for enhancing our understanding of air quality dynamics and improving predictive capabilities. This synergistic approach can help mitigate biases, enhance accuracy, and provide a more comprehensive view of atmospheric pollutants' distribution over this region.

https://doi.org/10.5194/egusphere-2024-959
Preprint. Discussion started: 6 May 2024

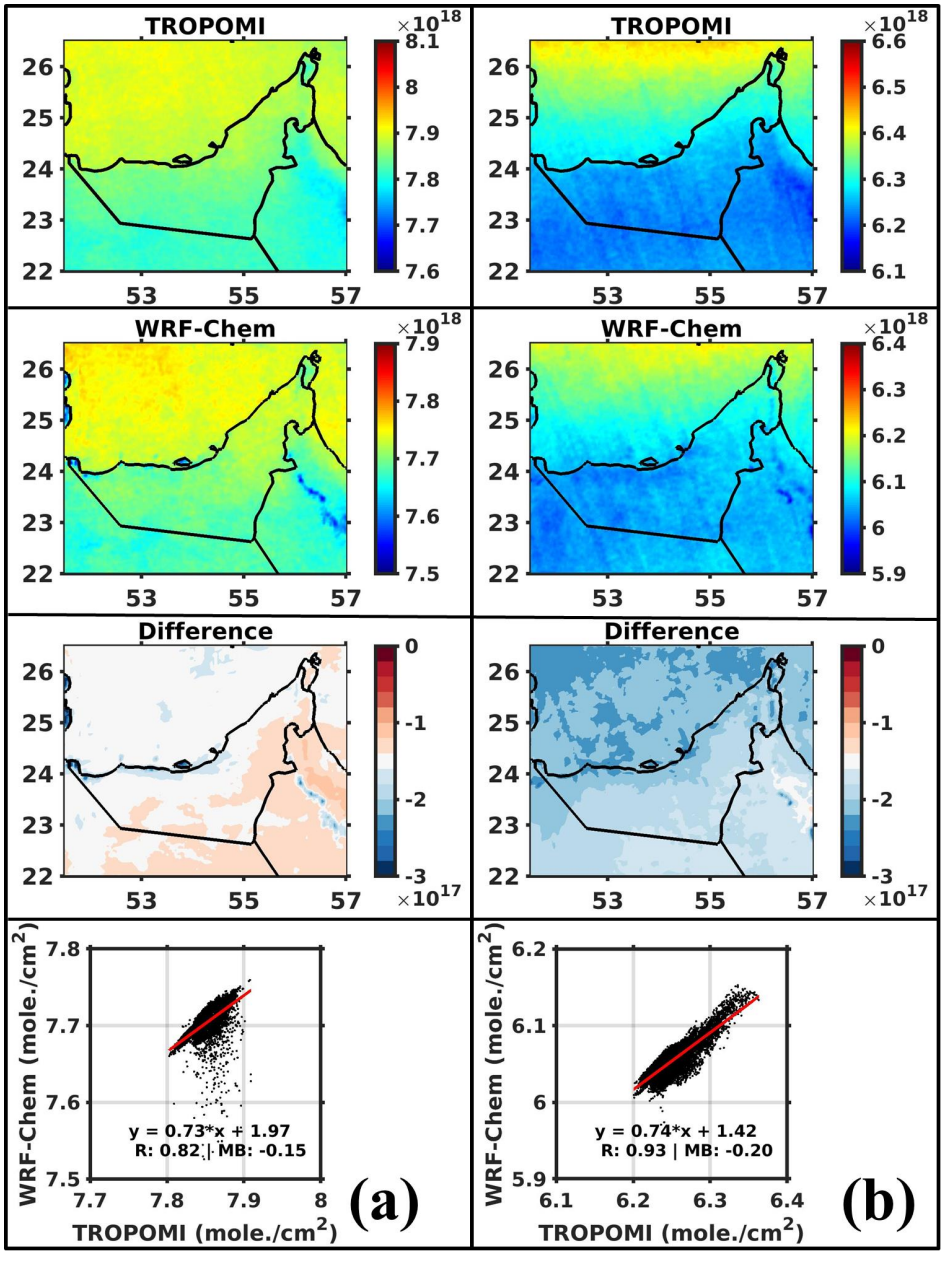

761

762 **Figure 7: Evaluation of WRF-Chem against satellite-derived O_3:** Same as Fig. 5 but for total column
763 of ozone.

764

765

https://doi.org/10.5194/egusphere-2024-959
Preprint. Discussion started: 6 May 2024

Table 5: Statistical verification scores for evaluation against TROPOMI measurements: skill scores between TROPOMI columns (mole. /cm^2), tropospheric column NO_2 (TROPOMI-NO_2), total column carbon monoxide (TROPOMI-CO) and total column ozone (TROPOMI-O_3) with corresponding WRF-chem simulated columns during June and December of 2018 over UAE. Means and MB, MAE and RMSE are given in units of ($x10^{15}$ mole. / cm^2 for TROPOMI-NO_2.

Parameter	Month	MOD	SAT	MB	MAE	R	RMSE
NO_2 ($x10^{16}$)	June	0.46	0.21	0.25	0.25	0.95	0.10
	Dec	0.43	0.24	0.19	0.20	0.94	0.12
O_3 ($x10^{18}$)		7.70	7.85	-0.15	0.15	0.82	0.01
		6.06	6.25	-0.2	0.20	0.93	0.01
CO ($x10^{18}$)		2.35	1.87	0.48	0.48	0.71	0.04
		0.76	1.89	-1.13	1.13	0.86	0.02

5. Conclusions

This study rigorously evaluates the performance of the Weather Research and Forecasting model coupled with chemistry (WRF-Chem). The model ability to simulate meteorological parameters and gaseous pollutants over the United Arab Emirates (UAE) is assessed during June and December 2018 to reflect contrasting summer and winter conditions. The model performance is assessed through comparison with ground-based observations and ERA-5 reanalysis data for meteorological parameters, and TROPOMI satellite observations for gaseous pollutants.

We evaluated WRF-Chem model's accuracy in simulating meteorological parameters, in particular 2-meter temperature (T2m), 10-meter wind speed (WS10m), and solar radiation (SR), across 16 locations in the UAE. The model generally underestimates T2m in summer by less than 0.5 °C and overestimates it in winter by less than 1.3 °C, with correlation coefficients ranging from 0.7 to 0.9 among the stations. WRF-chem performance for WS10m and SR has shown high scores, indicating enhanced accuracy across the locations. Regionally, it slightly underpredicts T2m in summer (by 0.37 °C for land and 0.48 °C for marine) mainly due to colder nights, and overestimates in winter (by 0.76 °C for land and 1.30 °C for marine), both with strong correlations above 0.83. Higher SR values in summer and winter, suggest reduced

https://doi.org/10.5194/egusphere-2024-959
Preprint. Discussion started: 6 May 2024

cloud cover and aerosol loading in WRF-Chem. For WS10m, the model's bias is within ±1 m/s, and correlation coefficients range between 0.78 and 0.89, indicating good agreement for both land and marine areas.

The comparison of ERA5 reanalysis data with WRF-Chem simulations revealed regional variations in T2m, specifically underestimation in the UAE's south and overestimation in the north-west. The most significant differences were observed over the Arabian Gulf region, especially during warmer months. These temperature discrepancies are crucial for the land-sea breeze circulation, with higher Gulf temperatures potentially weakening this pattern. This could lead to diminished transport of cleaner marine air inland, thereby hindering pollutant dispersion over land and adversely affecting air quality and pollutant distribution. Statistical metrics for summer shows an overestimation of 0.08 °C and a correlation coefficient (r) of 0.97, while winter's follows a similar pattern with an overestimation of 0.53 °C and r of 0.98 over land mass region of UAE. The fact that WRF-Chem performs well against in-situ data and ERA5 reanalysis with respect to air temperature is an indication the reanalysis dataset performs well in this region. The mean PBL from ERA5 is largely consistent with that from the WRF-Chem outputs, with both data sets displaying a clear seasonal variation—increased PBL during summer and decreased in winter, correlating with temperature changes. June's modelled PBL has a correlation of 0.91, and December's correlation of 0.98 with ERA5.

Regarding gaseous pollutants, both WRF-Chem and satellite data show higher TROPOMI-NO_2 columns greater than $12x10^{15}$ molecules/cm^2 in urban and industrial regions such as Dubai, Abu Dhabi and Ras Al Khaimah emirate, and reflecting emissions from economic activities like power generation, water desalination and industries. Lower concentrations of less than $5x10^{15}$ molecules/cm^2 are noted in less urbanized areas. The WRF-Chem model closely reproduces TROPOMI-NO_2 spatial patterns. However, it overestimates NO_2 in the Abu Dhabi region and underestimates it in north-eastern UAE. High correlation coefficients (0.95 in summer and 0.94 in winter) confirm the model's effectiveness in capturing NO_2's day-to-day variability. The model shows minimal MB and high r values, indicating small discrepancies in NO_2 estimations. Moreover, the WRF-Chem underestimates TROPOMI-O_3 columns, as indicated by negative MB values, yet maintains high correlation coefficients (0.82 in summer and 0.93 in winter), suggesting accurate ozone concentration simulations. TROPOMI-CO column simulations, however, exhibit significant discrepancies and lower correlation coefficients (0.71 in summer and 0.86 in winter), highlighting challenges in accurately

https://doi.org/10.5194/egusphere-2024-959
Preprint. Discussion started: 6 May 2024

modelling CO levels. This analysis stresses the WRF-Chem model's strengths in simulating NO_2 and O_3 columns with high fidelity to TROPOMI observations but also points out its limitations in estimating CO columns accurately.

The WRF-Chem model exhibits satisfactory capability in simulating key meteorological parameters and gaseous pollutants over the UAE, showcasing significant improvements in regional-scale dynamics. This is evidenced by strong correlation coefficients, variable MB, RMSE and MAE values, and a clear enhancement over previous research outcomes. This comprehensive assessment validates the model's effectiveness and identifies potential areas for improvement in simulating gaseous pollutant concentrations across the UAE. The discrepancies between model simulations and various observational data sets may arise from improper emission inventories, particularly anthropogenic emissions, model parameterizations, and meteorological inputs. Integrating model predictions with satellite observations and ground-based measurements is crucial for advancing air quality monitoring and enhancing the predictive accuracy of atmospheric pollutant distributions in the UAE. This collective approach aids in addressing biases and improving the overall understanding of regional air quality dynamics.

Code and Data Availability

The authors would like to thank the United Arab Emirates' National Center of Meteorology for providing meteorological observations at 16 weather stations for the months of June and December 2018 under an agreement with clauses for non-disclosure of data. Access to these data is restricted and readers should request them through contacting research@ncms.ae. The remaining products considered in this study are freely available online: (i) ERA-5 reanalysis data is extracted from the Copernicus Climate Change Service Climate Data Store (Hersbach et al. 2023a,b); (ii) Nitrogen Dioxide (NO_2), Ozone (O_3) and Carbon Monoxide (CO) column concentrations estimated from the measurements collected by the Tropopsheric Monitoring Instrument (TROPOMI) onboard the Sentinel 5-P satellite are extracted from the National Aeronautics and Space Administration's (NASA's) website; (iii) National Centers for Environmental Prediction (NCEP) Final (FNL) Operational Global Analysis meteorological data used to drive the WRF-chem simulations is downloaded from the National Center for Atmospheric Research (NCAR) Research Data Archive website (NCEP/NWS/NOAA/USDC, 2000), with the chemistry data used to force WRF-Chem, the ouput of the Community

https://doi.org/10.5194/egusphere-2024-959
Preprint. Discussion started: 6 May 2024

Atmosphere Model with Chemistry (CAM-chem) model, extracted from NCAR's website (Bucholz et al., 2019); (iv) the WRF-Chem model used, version 4.3.1, is freely available from the developers' website (WRF, 2023), with the pre-processor tools available at NCAR's website (NCAR, 2023). All figures displayed in this manuscript were generated with the Matrix Laboratory (MATLAB) software version 2023 (Mathworks, 2023).

Acknowledgment

We are thankful to the development team of the WRF-Chem model for making this model available as an open-source resource for research. We acknowledge the use of WRF-Chem pre-processor tools including mozbc, anthro_emiss, and bio_emiss provided by the Atmospheric Chemistry Observations and Modelling Lab (ACOM) of the National Center for Atmospheric Research (NCAR). Our also thanks go to the Community Atmosphere Model with Chemistry (CAM-Chem) for the chemical initial and boundary conditions. In addition, we are also thankful to the National Centers for Environmental Prediction (NCEP) Final (FNL) Operational Global Analysis data for supplying meteorological initial and lateral boundary conditions. Additionally, we are grateful to Sentinel-5P TROPOMI for satellite datasets. Finally, this research greatly benefited from the high-performance computing and research computing resources provided by Khalifa University. We express our sincere gratitude for their invaluable support.

Conflict of interest

The authors declare they do not have any conflict of interest.

Author contribution

Conceptualisation and methodology: D.F. and Y.Y.; Data curation and visualization: Y.Y.; formal analysis and interpretation: Y.Y., R.F., N.N., and D.F.; project administration and supervision: D.F.; writing—original draft: Y.Y.; review and editing: all authors.

References

Abdallah, C., Afif, C., El Masri, N., Öztürk, F., Keleş, M., & Sartelet, K. (2018). A first annual assessment of air quality modeling over Lebanon using WRF/Polyphemus. In *Atmospheric Pollution Research* (Vol. 9, Issue 4, pp. 643–654). Elsevier B.V. https://doi.org/10.1016/j.apr.2018.01.003

https://doi.org/10.5194/egusphere-2024-959
Preprint. Discussion started: 6 May 2024

Abida, R., Addad, Y., Francis, D., Temimi, M., Nelli, N., Fonseca, R., Nesterov, O., & Bosc, E. (2022). Evaluation of the Performance of the WRF Model in a Hyper-Arid Environment: A Sensitivity Study. *Atmosphere*, *13*(6). https://doi.org/10.3390/atmos13060985

Abuelgasim, A., & Farahat, A. (2020). Effect of dust loadings, meteorological conditions, and local emissions on aerosol mixing and loading variability over highly urbanized semiarid countries: United Arab Emirates case study. *Journal of Atmospheric and Solar-Terrestrial Physics*, *199*. https://doi.org/10.1016/j.jastp.2020.105215

Archer-Nicholls, S., Lowe, D., Darbyshire, E., Morgan, W. T., Bela, M. M., Pereira, G., Trembath, J., Kaiser, J. W., Longo, K. M., Freitas, S. R., Coe, H., & McFiggans, G. (2015). Characterising Brazilian biomass burning emissions using WRF-Chem with MOSAIC sectional aerosol. *Geoscientific Model Development*, *8*(3), 549–577. https://doi.org/10.5194/gmd-8-549-2015

Badia, A., & Jorba, O. (2015). Gas-phase evaluation of the online NMMB/BSC-CTM model over Europe for 2010 in the framework of the AQMEII-Phase2 project. *Atmospheric Environment*, *115*, 657–669. https://doi.org/10.1016/j.atmosenv.2014.05.055

Baldasano, J. M., Pay, M. T., Jorba, O., Gassó, S., & Jiménez-Guerrero, P. (2011). An annual assessment of air quality with the CALIOPE modeling system over Spain. *Science of the Total Environment*, *409*(11), 2163–2178. https://doi.org/10.1016/j.scitotenv.2011.01.041

Basha, G., Kishore, P., Ratnam, M. V., Ravindra Babu, S., Velicogna, I., Jiang, J. H., & Ao, C. O. (2019). Global climatology of planetary boundary layer top obtained from multi-satellite GPS RO observations. *Climate Dynamics*, *52*(3–4), 2385–2398. https://doi.org/10.1007/s00382-018-4269-1

Boersma, K. F., Eskes, H. J., Richter, A., De Smedt, I., Lorente, A., Beirle, S., Van Geffen, J. H. G. M., Zara, M., Peters, E., Van Roozendael, M., Wagner, T., Maasakkers, J. D., Van Der A, R. J., Nightingale, J., De Rudder, A., Irie, H., Pinardi, G., Lambert, J. C., & Compernolle, S. C. (2018). Improving algorithms and uncertainty estimates for satellite NO2 retrievals: Results from the quality assurance for the essential climate variables (QA4ECV) project. *Atmospheric Measurement Techniques*, *11*(12), 6651–6678. https://doi.org/10.5194/amt-11-6651-2018

Borsdorff, T., Aan de Brugh, J., Hu, H., Aben, I., Hasekamp, O., & Landgraf, J. (2018). Measuring Carbon Monoxide With TROPOMI: First Results and a Comparison With ECMWF-IFS Analysis Data. *Geophysical Research Letters*, *45*(6), 2826–2832. https://doi.org/10.1002/2018GL077045

Borsdorff, T., Hasekamp, O. P., Wassmann, A., & Landgraf, J. (2014). Insights into Tikhonov regularization: Application to trace gas column retrieval and the efficient calculation of total column averaging kernels. *Atmospheric Measurement Techniques*, *7*(2), 523–535. https://doi.org/10.5194/amt-7-523-2014

Branch, O., Schwitalla, T., Temimi, M., Fonseca, R., Nelli, N., Weston, M., Milovac, J., & Wulfmeyer, V. (2021). Seasonal and diurnal performance of daily forecasts with WRF V3.8.1 over the United Arab Emirates. *Geoscientific Model Development*, *14*(3), 1615–1637. https://doi.org/10.5194/gmd-14-1615-2021

Bucholz, R. R., Emmons, L. K., Tilmes, S., & The CESM2 Development Team (2019) CESM2.1/CAM-chem Instantaneous Output for Boundary Conditions. UCAR/NCAR – Atmospheric Chemistry Observations and Modeling Laboratory. Subset used (Lat: -5 to 50; Lon: 15 to 55; June and

December 2018) [Dataset]. Accessed on 10 July 2023, available online at https://doi.org/10.5065/NMP7-EP60

Chen, Y., Chen, S., Zhao, D., Li, J., Bi, H., Lou, G., & Guan, Y. (2022). The role of boundary layer height in India on transboundary pollutions to the Tibetan Plateau. *Science of the Total Environment*, *837*. https://doi.org/10.1016/j.scitotenv.2022.155816

Chin, M., Ginoux, P., Kinne, S., Torres, O., Holben, B. N., Duncan, B. N., Martin, R. V, Logan, J. A., Higurashi, A., & Nakajima, T. (2002). *Tropospheric Aerosol Optical Thickness from the GOCART Model and Comparisons with Satellite and Sun Photometer Measurements*. Accessed on 10 July 2023, available online at http://weather.engin.umich.edu/

Chudnovsky, A., Lyapustin, A., Wang, Y., Tang, C., Schwartz, J., & Koutrakis, P. (2014). High resolution aerosol data from MODIS satellite for urban air quality studies. *Central European Journal of Geosciences*, *6*(1), 17–26. https://doi.org/10.2478/s13533-012-0145-4

Coates, J., Mar, K. A., Ojha, N., & Butler, T. M. (2016). The influence of temperature on ozone production under varying NOx conditions - A modelling study. *Atmospheric Chemistry and Physics*, *16*(18), 11601–11615. https://doi.org/10.5194/acp-16-11601-2016

Crippa, M., Solazzo, E., Huang, G., Guizzardi, D., Koffi, E., Muntean, M., Schieberle, C., Friedrich, R., & Janssens-Maenhout, G. (2020). High resolution temporal profiles in the Emissions Database for Global Atmospheric Research. *Scientific Data*, *7*(1). https://doi.org/10.1038/s41597-020-0462-2

Dee, D. P., Uppala, S. M., Simmons, A. J., Berrisford, P., Poli, P., Kobayashi, S., Andrae, U., Balmaseda, M. A., Balsamo, G., Bauer, P., Bechtold, P., Beljaars, A. C. M., van de Berg, L., Bidlot, J., Bormann, N., Delsol, C., Dragani, R., Fuentes, M., Geer, A. J., … Vitart, F. (2011). The ERA-Interim reanalysis: Configuration and performance of the data assimilation system. *Quarterly Journal of the Royal Meteorological Society*, *137*(656), 553–597. https://doi.org/10.1002/qj.828

Dekker, Iris N., Sander Houweling, Sudhanshu Pandey, Maarten Krol, Thomas Röckmann, Tobias Borsdorff, Jochen Landgraf, and Ilse Aben. 2019. "What Caused the Extreme CO Concentrations during the 2017 High-Pollution Episode in India?" *Atmospheric Chemistry and Physics* 19 (6): 3433–45. https://doi.org/10.5194/acp-19-3433-2019.

German Aerospace Center (DLR), Copernicus Sentinel data processed by ESA (2020) Sentinel-5P TROPOMI Total Ozone Column 1-Orbit L2 5.5 km x 3.5 km. Greenbelt, MD, USA, Goddard Earth Sciences Data and Information Services Center (GES DISC) [Dataset]. Accessed on 10 October 2023, available online at https://doi.org/10.5270/S5P-ft13p57

Eltahan, M., Shokr, M., & Sherif, A. O. (2018). Simulation of severe dust events over egypt using tuned dust schemes in Weather Research Forecast (WRF-Chem). *Atmosphere*, *9*(7). https://doi.org/10.3390/atmos9070246

Emmons, L. K., Schwantes, R. H., Orlando, J. J., Tyndall, G., Kinnison, D., Lamarque, J. F., Marsh, D., Mills, M. J., Tilmes, S., Bardeen, C., Buchholz, R. R., Conley, A., Gettelman, A., Garcia, R., Simpson, I., Blake, D. R., Meinardi, S., & Pétron, G. (2020). The Chemistry Mechanism in the Community Earth System Model Version 2 (CESM2). *Journal of Advances in Modeling Earth Systems*, *12*(4). https://doi.org/10.1029/2019MS001882

Emmons, L. K., Walters, S., Hess, P. G., Lamarque, J., Pfister, G. G., Fillmore, D., Granier, C., & Emmons, L. K., Walters, S., Hess, P. G., Lamarque, J.-F., Pfister, G. G., Fillmore, D., Granier, C., Guenther, A., Kinnison, D., Laepple, T., Orlando, J., Tie, X., Tyndall, G., Wiedinmyer, C., Baughcum, S. L., and

https://doi.org/10.5194/egusphere-2024-959
Preprint. Discussion started: 6 May 2024

Kloster, S. (2010). Description and evaluation of the Model for Ozone and Related chemical Tracers, version 4 (MOZART-4). *Geoscientific Model Development*, *3*(1), 43–67. https://doi.org/10.5194/gmd-3-43-2010

Fonseca, R., & Francis, D. (2023). Satellite derived trends and variability of CO_2 concentrations in the Middle East during 2014–2023. *Frontiers in Environmental Science*, *11*. https://doi.org/10.3389/fenvs.2023.1289142

Fonseca, R., Francis, D., Nelli, N., & Thota, M. (2022). Climatology of the heat low and the intertropical discontinuity in the Arabian Peninsula. *International Journal of Climatology*, *42*(2), 1092–1117. https://doi.org/10.1002/joc.7291

Fonseca, R., Francis, D., Weston, M., Nelli, N., Farah, S., Wehbe, Y., Alhosari, T., Teixido, O., & Mohamed, R. (2021). Sensitivity of summertime convection to aerosol loading and properties in the united arab emirates. *Atmosphere*, *12*(12). https://doi.org/10.3390/atmos12121687

Fonseca, R., Temimi, M., Thota, M. S., Nelli, N. R., Weston, M. J., Suzuki, K., Uchida, J., Kumar, K. N., Branch, O., Wehbe, Y., Al Hosari, T., Al Shamsi, N., & Shalaby, A. (2020). On the analysis of the performance of WRF and nicam in a hyperarid environment. *Weather and Forecasting*, *35*(3), 891–919. https://doi.org/10.1175/WAF-D-19-0210.1

Francis, D., Fonseca, R., Nelli, N., Cuesta, J., Weston, M., Evan, A., & Temimi, M. (2020). The Atmospheric Drivers of the Major Saharan Dust Storm in June 2020. In *Geophysical Research Letters* (Vol. 47, Issue 24). Blackwell Publishing Ltd. https://doi.org/10.1029/2020GL090102

Francis, D., Fonseca, R., Nelli, N., Teixido, O., Mohamed, R., & Perry, R. (2022a). Increased Shamal winds and dust activity over the Arabian Peninsula during the COVID-19 lockdown period in 2020. *Aeolian Research*, *55*, 100786. https://doi.org/10.1016/j.aeolia.2022.100786

Francis, D., Nelli, N., Fonseca, R., Weston, M., Flamant, C., & Cherif, C. (2022b). The dust load and radiative impact associated with the June 2020 historical Saharan dust storm. *Atmospheric Environment*, *268*. https://doi.org/10.1016/j.atmosenv.2021.118808

Francis, D., Weston, M., Fonseca, R., Temimi, M., & Alsuwaidi, A. (2023). Trends and variability in methane concentrations over the Southeastern Arabian Peninsula. *Frontiers in Environmental Science*, *11*. https://doi.org/10.3389/fenvs.2023.1177877

Gao, Z., & Zhou, X. (2024). A review of the CAMx, CMAQ, WRF-Chem and NAQPMS models: Application, evaluation and uncertainty factors. *Environmental Pollution*, *343*, 123183. https://doi.org/10.1016/j.envpol.2023.123183

Geng, F., Zhao, C., Tang, X., Lu, G., & Tie, X. (2007). Analysis of ozone and VOCs measured in Shanghai: A case study. *Atmospheric Environment*, *41*(5), 989–1001. https://doi.org/10.1016/j.atmosenv.2006.09.023

Georgiou, G. K., Christoudias, T., Proestos, Y., Kushta, J., Hadjinicolaou, P., & Lelieveld, J. (2018). Air quality modelling in the summer over the eastern Mediterranean using WRF-Chem: Chemistry and aerosol mechanism intercomparison. *Atmospheric Chemistry and Physics*, *18*(3), 1555–1571. https://doi.org/10.5194/acp-18-1555-2018

Grell, G. a., Peckham, S. E., Schmitz, R., McKeen, S. a., Frost, G., Skamarock, W. C., & Eder, B. (2005). Fully coupled "online" chemistry within the WRF model. *Atmospheric Environment*, *39*(37), 6957–6975. https://doi.org/10.1016/j.atmosenv.2005.04.027

Griffin, D., Zhao, X., McLinden, C. A., Boersma, F., Bourassa, A., Dammers, E., Degenstein, D., Eskes, H., Fehr, L., Fioletov, V., Hayden, K., Kharol, S. K., Li, S. M., Makar, P., Martin, R. V., Mihele, C., Mittermeier, R. L., Krotkov, N., Sneep, M., … Wolde, M. (2019). High-Resolution Mapping of Nitrogen Dioxide With TROPOMI: First Results and Validation Over the Canadian Oil Sands. *Geophysical Research Letters*, *46*(2), 1049–1060. https://doi.org/10.1029/2018GL081095

Guenther, A. B., Jiang, X., Heald, C. L., Sakulyanontvittaya, T., Duhl, T., Emmons, L. K., & Wang, X. (2012). The model of emissions of gases and aerosols from nature version 2.1 (MEGAN2.1): An extended and updated framework for modeling biogenic emissions. *Geoscientific Model Development*, *5*(6), 1471–1492. https://doi.org/10.5194/gmd-5-1471-2012

Hersbach, H., Bell, B., Berrisford, P., Biavati, G., Horanyi, A., Munoz Sabater, J., Nicolas, J., Peubey, C., Radu, R., Rozum, I., Schepers, D., Simmons, A., Soci, C., Dee, D., & Thepaut, J.-N. (2023a) ERA5 hourly data on single levels from 1940 to present. Copernicus Climate Change Service Climate Data Store [Dataset]. Accessed on 14 November 2023, available online at https://doi.org/10.24381/cds.adbb2d47

Hersbach, H., Bell, B., Berrisford, P., Biavati, G., Horanyi, A., Munoz Sabater, J., Nicolas, J., Peubey, C., Radu, R., Rozum, I., Schepers, D., Simmons, A., Soci, C., Dee, D., & Thepaut, J.-N. (2023b) ERA5 hourly data on pressure levels from 1940 to present. Copernicus Climate Change Service Climate Data Store [Dataset]. Accessed on 14 November 2023, available online at https://doi.org/10.24381/cds.bd0915c6

Hersbach, H., Bell, B., Berrisford, P., Hirahara, S., Horányi, A., Muñoz-Sabater, J., Nicolas, J., Peubey, C., Radu, R., Schepers, D., Simmons, A., Soci, C., Abdalla, S., Abellan, X., Balsamo, G., Bechtold, P., Biavati, G., Bidlot, J., Bonavita, M., … Thépaut, J. N. (2020). The ERA5 global reanalysis. *Quarterly Journal of the Royal Meteorological Society*, *146*(730), 1999–2049. https://doi.org/10.1002/qj.3803

Hong, S. Y. (2010). A new stable boundary-layer mixing scheme and its impact on the simulated East Asian summer monsoon. *Quarterly Journal of the Royal Meteorological Society*, *136*(651), 1481–1496. https://doi.org/10.1002/qj.665

Hoshyaripour, G., Brasseur, G., Andrade, M. F., Gavidia-Calderón, M., Bouarar, I., & Ynoue, R. Y. (2016). Prediction of ground-level ozone concentration in São Paulo, Brazil: Deterministic versus statistic models. *Atmospheric Environment*, *145*, 365–375. https://doi.org/10.1016/j.atmosenv.2016.09.061

Hu, C., Kang, P., Jaffe, D. A., Li, C., Zhang, X., Wu, K., & Zhou, M. (2021). Understanding the impact of meteorology on ozone in 334 cities of China. *Atmospheric Environment*, *248*. https://doi.org/10.1016/j.atmosenv.2021.118221

Iacono, Michael J, Jennifer S Delamere, Eli J Mlawer, Mark W Shephard, Shepard A Clough, and William D Collins. 2008. "Radiative Forcing by Long-Lived Greenhouse Gases: Calculations with the AER Radiative Transfer Models." *Journal of Geophysical Research: Atmospheres* 113 (D13). https://doi.org/10.1029/2008JD009944

Ialongo, I., Virta, H., Eskes, H., Hovila, J., & Douros, J. (2020). Comparison of TROPOMI/Sentinel-5 Precursor NO2 observations with ground-based measurements in Helsinki. *Atmospheric Measurement Techniques*, *13*(1), 205–218. https://doi.org/10.5194/amt-13-205-2020

Ivatt, P. D., & Evans, M. J. (2020). Improving the prediction of an atmospheric chemistry transport model using gradient-boosted regression trees. *Atmospheric Chemistry and Physics*, *20*(13), 8063–8082. https://doi.org/10.5194/acp-20-8063-2020

Jena, C., Ghude, S. D., Kumar, R., Debnath, S., Govardhan, G., Soni, V. K., Kulkarni, S. H., Beig, G., & Nanjundiah, R. S. (2021). Performance of high resolution (400 m) P M 2 . 5 forecast over Delhi. *Scientific Reports*, *400 m*, 1–9. https://doi.org/10.1038/s41598-021-83467-8

Kain, J. S. (2004). The Kain-Fritsch Convective Parameterization: An Update. *Journal of Applied Meteorology*, *43*, 170–181. https://doi.org/10.1175/1520-0450(2004)043<0170:TKCPAU>2.0.CO;2

Karagulian, F., Temimi, M., Ghebreyesus, D., Weston, M., Kondapalli, N. K., Valappil, V. K., Aldababesh, A., Lyapustin, A., Chaouch, N., Al Hammadi, F., & Al Abdooli, A. (2019) Analysis of a severe dust storm and its impact on air quality conditions using WRF-Chem modeling, satellite imagery, and ground observations. *Air Quality, Atmosphere & Health*, *12*, 453-470. https://doi.org/10.1007/s11869-019-00674-z

Karumuri, R. K., Dasari, H. P., Gandham, H., Viswanadhapalli, Y., Madineni, V. R., & Hoteit, I. (2022). Impact of COVID-19 lockdown on the ambient air-pollutants over the Arabian Peninsula. *Frontiers in Environmental Science*, *10*. https://doi.org/10.3389/fenvs.2022.963145

Kerkweg, A., & Jöckel, P. (2012). The 1-way on-line coupled atmospheric chemistry model system MECO(n) - Part 1: Description of the limited-area atmospheric chemistry model COSMO/MESSy. *Geoscientific Model Development*, *5*(1), 87–110. https://doi.org/10.5194/gmd-5-87-2012

Kishta, M., Al Abadla, Z., Wahab, M. M. A., & Aldashti, H. (2023). Assessment of Heat Wave Indexing and Performance of ERA5 in Simulating Temperature and Precipitation Dataset over the UAE. *Environment Asia*, *16*(2), 48–65. https://doi.org/10.14456/ea.2023.20

Koninklijk Nederlands Meteorologisch Instituut (KNMI), Copernicus Sentinel data processed by ESA (2018) Sentinel-5P TROPOMI Tropospheric NO_2 1-Orbit L2 7 km x 3.5 km. Greenbelt, MD, USA, Goddard Earth Sciences Data and Information Services Center (GES DISC) [Dataset]. Accessed on 10 October 2023, available online at https://doi.org/10.5270/S5P-s4ljg54

Koninklijk Nederlands Meteorologisch Instituut/Netherlands Institute for Space Research (KNMI/SRON), Copernicus Sentinel data processed by ESA (2021) Sentinel-5P TROPOMI Tropospheric Carbon Monoxide CO 1-Orbit L2 5.5 km x 7 km. Greenbelt, MD, USA, Goddard Earth Sciences Data and Information Services Center (GES DISC) [Dataset]. Accessed on 10 October 2023, available online at https://doi.org/10.5270/S5P-bj3nry0

Koo, Y. S., Kim, S. T., Cho, J. S., & Jang, Y. K. (2012). Performance evaluation of the updated air quality forecasting system for Seoul predicting PM 10. *Atmospheric Environment*, *58*(3), 56–69. https://doi.org/10.1016/j.atmosenv.2012.02.004

Krol, M., Houweling, S., Bregman, B., Van Den Broek, M., Segers, A., Van Velthoven, P., Peters, W., Dentener, F., & Bergamaschi, P. (2005). The two-way nested global chemistry-transport zoom model TM5: algorithm and applications. In *Atmos. Chem. Phys* (Vol. 5). www.atmos-chem-phys.org/acp/5/417/SRef-ID:1680-7324/acp/2005-5-417EuropeanGeosciencesUnion

Kumar, R. (2011). Weather Research and Forecasting Model with Chemistry (WRF-CHEM) over South Asia. *Pubman.Mpdl.Mpg.De*. Accessed on 10 July 2023, available online at

http://pubman.mpdl.mpg.de/pubman/item/escidoc:994147:1/component/escidoc:994146/BzE_57.pdf

Kumar, R., Barth, M. C., Pfister, G. G., Delle Monache, L., Lamarque, J. F., Archer-Nicholls, S., … Walters, S. (2018). How Will Air Quality Change in South Asia by 2050? *Journal of Geophysical Research: Atmospheres*, *123*(3), 1840–1864. https://doi.org/10.1002/2017JD027357

Kumar, R., Bhardwaj, P., Pfister, G., Drews, C., Honomichl, S., & D'attilo, G. (2021). Description and evaluation of the fine particulate matter forecasts in the NCAR regional air quality forecasting system. *Atmosphere*, *12*(3). https://doi.org/10.3390/atmos12030302

Kumar, R., Naja, M., Pfister, G. G., Barth, M. C., Wiedinmyer, C., & Brasseur, G. P. (2012). Simulations over South Asia using the Weather Research and Forecasting model with Chemistry (WRF-Chem): Chemistry evaluation and initial results. *Geoscientific Model Development*, *5*(3), 619–648. https://doi.org/10.5194/gmd-5-619-2012

Labow, G. J., Ziemke, J. R., McPeters, R. D., Haffner, D. P., & Bhartia, P. K. (2015). A total ozone-dependent ozone profile climatology based on ozonesondes and Aura MLS data. *Journal of Geophysical Research*, *120*(6), 2537–2545. https://doi.org/10.1002/2014JD022634

Lambert, J.-C., A. Keppens, S. Compernolle, K.-U. Eichmann, M. de Graaf, D. Hubert, B. Langerock, A. Ludewig, M.K. Sha, T. Verhoelst, T. Wagner, C. Ahn, A. Argyrouli, D. Balis, K.L. Chan, M. Coldewey-Egbers, I. De Smedt, H. Eskes, A.M. Fjæraa, … M. Weber. (2023). *Quarterly Validation Report of the Copernicus Sentinel-5 Precursor Operational Data Products #21: April 2018-November 2023*.

Landgraf, J., Aan De Brugh, J., Scheepmaker, R., Borsdorff, T., Hu, H., Houweling, S., Butz, A., Aben, I., & Hasekamp, O. (2016). Carbon monoxide total column retrievals from TROPOMI shortwave infrared measurements. *Atmospheric Measurement Techniques*, *9*(10), 4955–4975. https://doi.org/10.5194/amt-9-4955-2016

Li, T. Y., Deng, X. J., Li, Y., Song, Y. S., Li, L. Y., Tan, H. B., & Wang, C. L. (2018). Transport paths and vertical exchange characteristics of haze pollution in Southern China. *Science of the Total Environment*, *625*, 1074–1087. https://doi.org/10.1016/j.scitotenv.2017.12.235

Li, Y., Gibson, J. M. D., Jat, P., Puggioni, G., Hasan, M., West, J. J., Vizuete, W., Sexton, K., & Serre, M. (2010). Burden of disease attributed to anthropogenic air pollution in the United Arab Emirates: Estimates based on observed air quality data. *Science of the Total Environment*, *408*(23), 5784–5793. https://doi.org/10.1016/j.scitotenv.2010.08.017

Liu, F., Tao, Z., Beirle, S., Joiner, J., Yoshida, Y., Smith, S. J., Knowland, K. E., & Wagner, T. (2022). A new method for inferring city emissions and lifetimes of nitrogen oxides from high-resolution nitrogen dioxide observations: A model study. *Atmospheric Chemistry and Physics*, *22*(2), 1333–1349. https://doi.org/10.5194/acp-22-1333-2022

Lu, X., Zhang, L., & Shen, L. (2019). Meteorology and Climate Influences on Tropospheric Ozone: a Review of Natural Sources, Chemistry, and Transport Patterns. In *Current Pollution Reports* (Vol. 5, Issue 4, pp. 238–260). Springer. https://doi.org/10.1007/s40726-019-00118-3

Madronich, S. (1987). Photodissociation in the atmosphere: 1. Actinic flux and the effects of ground reflections and clouds. *Journal of Geophysical Research: Atmospheres*, *92*(D8), 9740–9752. https://doi.org/https://doi.org/10.1029/JD092iD08p09740

https://doi.org/10.5194/egusphere-2024-959
Preprint. Discussion started: 6 May 2024

Manders, A. M. M., Builtjes, P. J. H., Curier, L., Gon, H. A. C. D. Vander, Hendriks, C., Jonkers, S., Kranenburg, R., Kuenen, J. J. P., Segers, A. J., Timmermans, R. M. A., Visschedijk, A. J. H., Kruit, R. J. W., Pul, W. A. J. V., Sauter, F. J., Van Der Swaluw, E., Swart, D. P. J., Douros, J., Eskes, H., Van Meijgaard, E., … Schaap, M. (2017). Curriculum vitae of the LOTOS-EUROS (v2.0) chemistry transport model. *Geoscientific Model Development*, *10*(11), 4145–4173. https://doi.org/10.5194/gmd-10-4145-2017

Mathworks (2023) MATLAB. Maths. Graphic. Programming [Software]. Accessed on 10 July 2023, available online at https://uk.mathworks.com/products/matlab.html

Menut, L., Bessagnet, B., Briant, R., Cholakian, A., Couvidat, F., Mailler, S., Pennel, R., Siour, G., Tuccella, P., Turquety, S., & Valari, M. (2021). The CHIMERE v2020r1 online chemistry-transport model. *Geoscientific Model Development*, *14*(11), 6781–6811. https://doi.org/10.5194/gmd-14-6781-2021

Morrison, H., Thompson, G., & Tatarskii, V. (2009). Impact of cloud microphysics on the development of trailing stratiform precipitation in a simulated squall line: Comparison of one- and two-moment schemes. *Monthly Weather Review*, *137*(3), 991–1007. https://doi.org/10.1175/2008MWR2556.1

National Center for Atmospheric Research (2023) Download WRF-CHEM Processors [Dataset]. Accessed on 10 July 2023, available online at https://www.acom.ucar.edu/wrf-chem/download.shtml

National Centers for Environmental Prediction/National Weather Service/National Oceanic and Atmospheric Administration/United States Department of Commerce (NCEP/NWS/NOAA/USDC) (2000) NCEP FNL Operational Model Global Tropospheric Analyses, continuing from July 1999. Research Data Archive at the National Center for Atmospheric Research, Computational and Information Systems Labotory [Dataset]. Accessed on 10 July 2023, available online at https://doi.org/10.5065/D6M043C6

Nelli, N., Fissehaye, S., Francis, D., Fonseca, R., Temimi, M., Weston, M., Abida, R., & Nesterov, O. (2021) Characteristics of atmospheric aerosols over the UEA inferred from CALIPSO and sun photometer aerosol optical depth. *Earth and Space Science*, *8*, e2020EA001360. https://doi.org/10.1029/2020EA001360

Nelli, N. R., Temimi, M., Fonseca, R. M., Weston, M. J., Thota, M. S., Valappil, V. K., Branch, O., Wulfmeyer, V., Wehbe, Y., Al Hosary, T., Shalaby, A., Al Shamsi, N., & Al Naqbi, H. (2020) Impact of roughness length on WRF simulated land-atmospheres interactions over a hyper-arid region. *Earth and Space Science*, *7*, e2020EA001165. https://doi.org/10.1029/2020EA001165

Nesterov, O., Temimi, M., Fonseca, R., Nelli, N. R., Addad, Y., Bosc, E., & Abida, R. (2021). Validation and statistical analysis of the Group for High Resolution Sea Surface Temperature data in the Arabian Gulf. *Oceanologia*, *63*(4), 497–515. https://doi.org/10.1016/j.oceano.2021.07.001

Nhu, T., Do, N., Ngo, X. T., Pham, V. H., Vuong, N. L., Le, H. A., & Pham, C. T. (2021). *Application of WRF-Chem to simulate air quality over Northern Vietnam*. *2016*, 12067–12081. https://doi.org/10.1007/s11356-020-08913-y

Parajuli, S. P., Stenchikov, G. L., Ukhov, A., & Kim, H. (2019). Dust Emission Modeling Using a New High-Resolution Dust Source Function in WRF-Chem With Implications for Air Quality. *Journal of*

https://doi.org/10.5194/egusphere-2024-959
Preprint. Discussion started: 6 May 2024

Geophysical Research: Atmospheres, *124*(17–18), 10109–10133. https://doi.org/10.1029/2019JD030248

Parajuli, Sagar P., Georgiy L. Stenchikov, Alexander Ukhov, Hugh Morrison, Illia Shevchenko, and Suleiman Mostamandi. 2023. Simulation of a Dust-And-Rain Event Across the Red Sea Using WRF-Chem. *Journal of Geophysical Research: Atmospheres* 128 (14). https://doi.org/10.1029/2022JD038384

Parajuli, Sagar P., Georgiy L. Stenchikov, Alexander Ukhov, Suleiman Mostamandi, Paul A. Kucera, Duncan Axisa, William I. Gustafson, and Yannian Zhu. 2022. Effect of Dust on Rainfall over the Red Sea Coast Based on WRF-Chem Model Simulations. *Atmospheric Chemistry and Physics* 22 (13): 8659–82. https://doi.org/10.5194/acp-22-8659-2022

Ramadan, E. (2015) Sustainable Urbanization in the Arabian Gulf Region: Problems and Challenges. *Arts and Social Sciences Journal*, *6:2*. https://doi.org/10.4172/2151-6200:10000109

Reddy, K. K., Naja, M., Ojha, N., Mahesh, P., & Lal, S. (2012). Influences of the boundary layer evolution on surface ozone variations at a tropical rural site in India. *Journal of Earth System Science*, *121*(4), 911–922. https://doi.org/10.1007/s12040-012-0200-z

Ritter, M., Müller, M. D., Tsai, M. Y., & Parlow, E. (2013). Air pollution modeling over very complex terrain: An evaluation of WRF-Chem over Switzerland for two 1-year periods. *Atmospheric Research*, *132–133*, 209–222. https://doi.org/10.1016/j.atmosres.2013.05.021

Schwitalla, T., Branch, O., & Wulfmeyer, V. (2020). Sensitivity study of the planetary boundary layer and microphysical schemes to the initialization of convection over the Arabian Peninsula. *Quarterly Journal of the Royal Meteorological Society*, *146*(727), 846–869. https://doi.org/10.1002/qj.3711

Shahbaz, M., Sbia, R., Hamdi, H., & Ozturk, I. (2014) Economic growth, electricity consumption, urbanization and environmental degradation relationship in United Arab Emirates. *Ecological Indicators*, *45*, 622-631. https://doi.org/10.1016/j.ecolind.2014.05.022

Shami, A. Al, Aawar, E. Al, Baayoun, A., Saliba, N. A., Kushta, J., Christoudias, T., & Lakkis, I. (2022). Updated national emission inventory and comparison with the Emissions Database for Global Atmospheric Research (EDGAR): case of Lebanon. *Environmental Science and Pollution Research*, *29*(20), 30193–30205. https://doi.org/10.1007/s11356-021-17562-8

Sicard, P., Crippa, P., De Marco, A., Castruccio, S., Giani, P., Cuesta, J., Paoletti, E., Feng, Z., & Anav, A. (2021). High spatial resolution WRF-Chem model over Asia: Physics and chemistry evaluation. *Atmospheric Environment*, *244*(June 2020), 118004. https://doi.org/10.1016/j.atmosenv.2020.118004

Sillman, S. (1999). The relation between ozone, NO V and hydrocarbons in urban and polluted rural environments. In *Atmospheric Environment*, *33*, 1821-1845. https://doi.org/10.1016/S1352-2310(98)00345-8

Skamarock WC, et al. (2008). A description of the advanced research WRF version 3, NCAR Tech. Note, NCAR/TN-468+STR. *Natl. Cent. for Atmos. Res. Boulder, Colorado*, *June*, 408. https://doi.org/10.5065/D68S4MVH

Srinivas, R., Panicker, A. S., Parkhi, N. S., Peshin, S. K., & Beig, G. (2016). Sensitivity of online coupled model to extreme pollution event over a mega city Delhi. *Atmospheric Pollution Research*, *7*(1), 25–30. https://doi.org/10.1016/j.apr.2015.07.001

Temimi, M., Fonseca, R., Nelli, N., Weston, M., Thota, M., Valappil, V., Branch, O., Wizemann, H., Kumar Kondapalli, N., Wehbe, Y., Hosary, T. AL, Shalaby, A., Shamsi, N. AL, & Naqbi, H. AL. (2020a). Assessing the Impact of Changes in Land Surface Conditions on WRF Predictions in Arid Regions. *Journal of Hydrometeorology*. https://doi.org/10.1175/JHM-D-20

Temimi, M., Fonseca, R., Nelli, N., Weston, M., Thota, M., Valappil, V., Branch, O., Wizemann, H., Kumar Kondapalli, N., Wehbe, Y., Hosary, T. AL, Shalaby, A., Shamsi, N. AL, & Naqbi, H. AL. (2020b). Assessing the Impact of Changes in Land Surface Conditions on WRF Predictions in Arid Regions. *Journal of Hydrometeorology*, 2829–2853. https://doi.org/10.1175/JHM-D-20-0083.1

Tewari, M., Chen, F., Wang, W., Dudhia, J., Lemone, M. A., Mitchell, K., Ek, M., Gayno, G., Wegiel, J., & Cuenca, R. H. (2004). *Implementation and verification of the united NOAH land surface model in the WRF model*. https://www2.mmm.ucar.edu/wrf/users/physics/phys_refs/LAND_SURFACE/noah.pdf

Tie, X. (2003). Effect of clouds on photolysis and oxidants in the troposphere. *Journal of Geophysical Research*, *108*(D20). https://doi.org/10.1029/2003jd003659

Tie, X., Brasseur, G., Emmons, L., Horowitz, L., & Kinnison, D. (2001). Effects of aerosols on tropospheric oxidants: A global model study. *Journal of Geophysical Research*, *106*(D19), 22931. https://doi.org/10.1029/2001JD900206

Ukhov, A., Ahmadov, R., Grell, G., & Stenchikov, G. (2021). Improving dust simulations in WRF-Chem v4.1.3 coupled with the GOCART aerosol module. *Geoscientific Model Development*, *14*(1), 473–493. https://doi.org/10.5194/gmd-14-473-2021

Van Geffen, J. H. G. M., Eskes, H. J., Boersma, K. F., & Veefkind, J. P. (2022). *TROPOMI ATBD of the total and tropospheric NO 2 data products document number : S5P-KNMI-L2-0005-RP*. Accessed on 10 July 2023, available online at https://sentinel.esa.int/documents/247904/2476257/sentinel-5p-tropomi-atbd-no2-data-products

Veefkind, J. P., Aben, I., McMullan, K., Förster, H., de Vries, J., Otter, G., Claas, J., Eskes, H. J., de Haan, J. F., Kleipool, Q., van Weele, M., Hasekamp, O., Hoogeveen, R., Landgraf, J., Snel, R., Tol, P., Ingmann, P., Voors, R., Kruizinga, B., … Levelt, P. F. (2012). TROPOMI on the ESA Sentinel-5 Precursor: A GMES mission for global observations of the atmospheric composition for climate, air quality and ozone layer applications. *Remote Sensing of Environment*, *120*, 70–83. https://doi.org/10.1016/j.rse.2011.09.027

Veefkind,, Keppens, A., & de Haan, J. (2021). *TROPOMI ATBD Ozone Profile*. Accessed on 10 July 2023. Available online at https://sentinel.esa.int/documents/247904/2476257/Sentinel-5P-TROPOMI-ATBD-Ozone-Profile.pdf

Waked, A., Afif, C., & Seigneur, C. (2012). An atmospheric emission inventory of anthropogenic and biogenic sources for Lebanon. *Atmospheric Environment*, *50*, 88–96. https://doi.org/10.1016/j.atmosenv.2011.12.058

Wang, Y., Bai, Y., Zhi, X., Wu, K., Zhao, T., Zhou, Y., Xiong, J., Zhu, S., Zhou, W., Hu, W., Zhang, L., & Meng, K. (2022). Two Typical Patterns of Regional PM2.5 Transport for Heavy Air Pollution Over

https://doi.org/10.5194/egusphere-2024-959
Preprint. Discussion started: 6 May 2024

Central China: Rapid Transit Transport and Stationary Accumulation Transport. *Frontiers in Environmental Science*, *10*. https://doi.org/10.3389/fenvs.2022.890514

WRF (2023) Weather Research and Forecasting model [Model]. Accessed on 10 July 2023, available online at https://github.com/wrf-model/WRF/releases

Wehbe, Y., Ghebreyesus, D., Temimi, M., Milewski, A., & Al Mandous, A. (2017). Assessment of the consistency among global precipitation products over the United Arab Emirates. *Journal of Hydrology: Regional Studies*, *12*, 122–135. https://doi.org/10.1016/j.ejrh.2017.05.002

Wesely, M. L. (1989). Parameterization of surface resistance to gaseous dry deposition in regional numerical model. *Atmospheric Environment*, *23*(6), 1293–1304. https://doi.org/10.1016/0004-6981(89)90153-4

Wizenberg, T., Strong, K., Walker, K., Lutsch, E., Borsdorff, T., & Landgraf, J. (2021). Intercomparison of CO measurements from TROPOMI, ACE-FTS, and a high-Arctic ground-based Fourier transform spectrometer. *Atmospheric Measurement Techniques*, *14*(12), 7707–7728. https://doi.org/10.5194/amt-14-7707-2021

Yarragunta, Y., Srivastava, S., Mitra, D., & Chandola, H. C. (2021). Source apportionment of carbon monoxide over India: a quantitative analysis using MOZART-4. *Environmental Science and Pollution Research*, *28*(7), 8722–8742. https://doi.org/10.1007/s11356-020-11099-y

Yarragunta, Y., Srivastava, S., Mitra, D., & Chandola, H. C. H. C. (2020). Influence of forest fire episodes on the distribution of gaseous air pollutants over Uttarakhand, India. *GIScience and Remote Sensing*, *57*(2), 190–206. https://doi.org/10.1080/15481603.2020.1712100

Yarragunta, Y., Srivastava, S., Mitra, D., Le Flochmoën, E., Barret, B., Kumar, P., & Chandola, H. C. C. (2019). Source attribution of carbon monoxide and ozone over the Indian subcontinent using MOZART-4 chemistry transport model. *Atmospheric Research*, *227*(April), 165–177. https://doi.org/10.1016/j.atmosres.2019.04.019

Yin, H., Lu, X., Sun, Y., Li, K., Gao, M., Zheng, B., & Liu, C. (2021). Unprecedented decline in summertime surface ozone over eastern China in 2020 comparably attributable to anthropogenic emission reductions and meteorology. *Environmental Research Letters*, *16*(12). https://doi.org/10.1088/1748-9326/ac3e22

Zhang, Y., Bocquet, M., Mallet, V., Seigneur, C., & Baklanov, A. (2012). Real-time air quality forecasting, part I: History, techniques, and current status. *Atmospheric Environment*, *60*, 632–655. https://doi.org/10.1016/j.atmosenv.2012.06.031

Zhang, Y., Pan, Y., Wang, K., Fast, J. D., & Grell, G. A. (2010). WRF/Chem-MADRID: Incorporation of an aerosol module into WRF/Chem and its initial application to the TexAQS2000 episode. *Journal of Geophysical Research Atmospheres*, *115*(18). https://doi.org/10.1029/2009JD013443

Zhang, Xu, X., & Su, Y. (2020). Impacts of regional transport and meteorology on ground-level ozone in windsor, canada. *Atmosphere*, *11*(10). https://doi.org/10.3390/atmos11101111